Title
INTERACTIONS OF FAST ELECTRONS AND POSITRONS WITH MATTER

Author
Violet, Charles E.

Publication Date
1953-04-03

UNIVERSITY OF CALIFORNIA — BERKELEY

RADIATION LABORATORY

DISCLAIMER

UCRL-2163
Unclassified-Physics Distribution

UNIVERSITY OF CALIFORNIA

Radiation Laboratory

Contract No. W-7405-eng-48

INTERACTIONS OF FAST ELECTRONS AND POSITRONS WITH MATTER

Charles E. Violet
(Thesis)

April 3, 1953

Berkeley, California

TABLE OF CONTENTS

INTERACTIONS OF FAST ELECTRONS AND POSITRONS WITH MATTER

Charles E. Violet

ABSTRACT

From observations of high energy electron and positron tracks in nuclear emulsion, the following processes were studied: (1) electron-electron scattering, (2) positron-electron scattering, (3) the ratio of plateau to minimum grain density for electrons, (4) nuclear scattering of electrons and positrons, (5) positron annihilation in flight, (6) pair production by electrons and positrons, and (7) inelastic electron-electron and positron-electron collisions. Experimental results pertaining to (1), (2), (4), (5), and (6) are consistent with the appropriate theories. The ratio of (3) is found to be 1.087 ± 0.010. Process (7) was not detected.

INTERACTIONS OF FAST ELECTRONS AND POSITRONS WITH MATTER

Charles E. Violet

I INTRODUCTION

Present day quantum electrodynamics unified with particle mechanics is a consistent scheme which, in the first approximation, is capable of describing a wide range of phenomena. The known experimental behavior of the electron and positron is completely described by this theory. The bulk of the existing experimental knowledge of these particles has been obtained from experiments involving energies of only a few Mev or less. Recent cosmic ray investigations indicate that the theory might be valid at high energies. There is yet a need, however, for the experimental study of high energy electron and positron processes in some detail. It is with the objective of giving a clearer picture of these high energy processes that the present investigation has been undertaken.

A consequence of the perfection of nuclear track emulsions capable of recording minimum ionization tracks was the possibility of employing this technique to study the interactions of fast electrons and positrons with matter. In observing the tracks of these particles with the aid of a microscope, one would expect to study the following:

1. Elastic electron-electron scattering
2. Elastic positron-electron scattering
3. Energy loss by ionization
4. Nuclear scattering of positrons and electrons
5. Positron annihilation in flight
6. Pair production
7. Inelastic electron-electron and positron-electron collisions
8. Multiple scattering

The method of following a track as it penetrates the emulsion enables one to observe directly all important processes except the energy loss by radiation.

In what follows we shall investigate the scattering of positrons and electrons by electrons at primary energies of ~ 174 Mev, and the nuclear scattering of ~ 39 Mev positrons and electrons. A comparison will be made of the grain density and hence the energy loss by ionization of 2.8 Mev and 293 Mev electrons. For the more rare events of pair production and annihilation, orders of magnitude of the respective cross sections will be given. Multiple scattering will not be studied per se. The multiple scattering of primary particles was measured to determine their mean energy in emulsion and the spread of primary energies about the mean.

II EXPERIMENTAL PROCEDURE

A. Exposures

Two-hundred micron Ilford G-5 plates were exposed to electrons and positrons of discrete energies obtained by magnetic separation in the pair spectrometer at the Berkeley synchrotron (Figures 1 and 2). The magnetic field was initially calibrated as a function of field current by measuring the field with a proton moment device. The leading edge of the plates were well within the homogeneous field. The field direction was determined by the force on a current carrying conductor. The magnetic field current (107.5 amps.) was checked during exposures with a Leeds and Northrup potentiometer. By means of a telescope, the axis of symmetry of the apparatus (Figure 1) was aligned with the synchrotron beam.

The plates were exposed so that electrons from the target entered the emulsion at a slight angle ($\sim 5^{\circ}$) to the surface and perpendicular to the leading edge of the plate. In order to insure that only electrons which came directly from the converter were accepted, only tracks whose initial directions lay within $\pm 2\,1/2^{\circ}$ of the perpendicular were scanned. This criterion included over ninety percent of all high energy electron tracks in the emulsion irrespective of direction. On plates exposed with no converter in the beam a number of acceptable tracks were found which was less than one percent of that found on plates exposed with the converter in the beam.

Immediately following the exposure of some plates to three-hundred Mev electrons, these same plates were exposed to 3 Mev electrons obtained by magnetic analysis of an electron linear accelerator beam. To minimize air scattering of the 3 Mev electrons, an enclosed brass channel lined with polyethylene was constructed to provide a nearly air-free path from accelerator to plate (Figures 3 and 4). Care was taken in the design to minimize the possibility of accepting electrons scattered from the interior walls. During exposure, the pressure in the channel was ~ 0.02 mm.

B. Eradication and Development

Due to the high background of electron tracks usually present in all but freshly prepared electron sensitive emulsions, it is usually necessary to eradicate the latent image of old tracks immediately before exposure. Fading of the latent image under certain conditions of temperature and humidity has been a commonly observed phenomena in photography. Yagoda and Kaplan[1], by storing plates in a water-saturated atmosphere at 35° C, succeeded in producing a controlled acceleration of this fading property. Their study was concerned with tracks of heavy particles in fine grain emulsion. At this time it was not known whether this technique could be applied to electron tracks in a coarse grain emulsion such as Ilford G-5. In the present experiment, eradication was deemed necessary in order that an electron-electron or positron-electron scatter could be observed unambiguously. A successful eradication procedure was subsequently developed.

Plates supported by stainless steel wires secured to a lucite frame (Figures 5 and 6) were sealed in an enameled box. This assemblage was immersed in a water bath thermostatically maintained at $97^{\circ} \pm 1^{\circ}$ F. The relative humidity was maintained at 100 percent by including a wet sponge in the box with the plates. Two-hundred micron Ilford G-5 emulsions, stored in this way for seventy-two hours, were developed without drying with uneradicated plates of the same batch. Comparison of the background on the two sets of plates led to the conclusion that practically all electron tracks could be removed in this way. Comparison of developed minimum ionization tracks in such eradicated plates and uneradicated plates of the same batch indicated no noticeable difference in grain density. After eradication the plates were dried in a light-tight box in the presence of a gentle flow of air supplied by a fan.

Immediately following exposure the plates were developed by a temperature cycle process[2] in order to obtain uniform and highly sensitive development. (Appendix I).

Chronologically, the first part of the present work was a study of the scattering of $\sim$174 Mev electrons and positrons. Data on these were obtained from plates which were eradicated and developed

in the manner described above. These emulsions were over developed, by some standards, in order to minimize the possibility of missing a scattering event. The grain density of the primary tracks was 41.9 ± 1.0 grains/100 microns. Unfortunately, recent batches of G-5's received from Ilford suffer a serious loss of sensitivity (by a factor of $\sim 1/3$) when subjected to the described eradication and development. In the absence of any eradication, minimum ionization tracks in these later batches of emulsions had a grain density of ~ 25 grains/100 microns for the same development. An attempt was made to improve this state of affairs by a change in development to the "Bristol method"[4] (Appendix II). However, this resulted in a grain density approximately the same as before. Fortunately, in the study of nuclear scattering and grain densities the existance of background tracks does not interfere with the analysis. Thus, most of the work on these topics was done with uneradicated Ilford G-5 emulsions developed by the "Bristol method".

III ELECTRON-ELECTRON AND POSITRON-ELECTRON SCATTERING

A. Theory and Experiment

1. Electron-Electron Scattering

The elastic collision of two free electrons has been considered from a theoretical viewpoint by several authors[4,5,6,7]. The most complete treatment is due to Møller who gives the differential scattering cross section as:

$$\sigma(\theta^*)d\theta^* = \frac{(\gamma_o + 1)\,\pi r_o^{\,2} \sin\theta^* d\theta^*}{\gamma_o^{\,2}\,\beta_o^{\,4}} \left[\csc^4\frac{\theta^*}{2} + \sec^4\frac{\theta^*}{2} - \csc^2\frac{\theta^*}{2}\sec^2\frac{\theta^*}{2} + \frac{(\gamma_o - 1)^2}{\gamma_o^{\,2}}(1 + 4\csc^2\theta^*)\right] \qquad (1)$$

where θ^* is the center of mass scattering angle, r_o is the classical electron radius, $\beta_o = v_o/c$, $\gamma_o = (1 - \beta_o^2)^{-1/2}$ and v_o is the velocity of the incident electron in the rest frame of the other electron (the laboratory system).

The sum of the first two terms corresponds to the classical cross section for Rutherford scattering when no identification is made among the primary and scattered particles, and will be termed the "relativistic Rutherford equation". The third term represents the interference between the first two terms arising from the quantum mechanical treatment of the scattering of identical particles[5]. The sum of the first three terms resemble Mott's original formulation and is referred to as the "relativistic Mott equation". The fourth term is the relativistic correction introduced by Møller[6] and represents the effect of retardation and spin interaction.

Equation (1) may be expressed in terms of the parameter A, defined as the ratio of the kinetic energy of the secondary or knock-on electron to the kinetic energy of the primary electron in the laboratory system. It is not possible to identify the primary electron with either secondary electron. The knock-on electron is defined as the secondary

electron of lower kinetic energy. The maximum value of A is thus 0.5. By a simple transformation as shown by Møller, Equation (1) becomes:

$$\sigma(A)dA = \frac{2\pi r_o^2}{\beta_o^2 (\gamma_o - 1)} \left[\frac{1}{A^2 (1 - A)^2} - \frac{3}{A (1 - A)} + \frac{(\gamma_o - 1)^2}{\gamma_o^2} \left(1 + \frac{1}{A (1 - A)} \right) \right] dA \qquad (2)$$

The corresponding relativistic Rutherford cross section is:

$$\sigma(A)dA = \frac{2\pi r_o^2}{\beta_o^2 (\gamma_o - 1)} \left[\frac{1}{A^2 (1 - A)^2} - \frac{2}{A (1 - A)} \right] dA \qquad (3)$$

The relativistic Mott cross section is:

$$o(A)dA = \frac{2\pi r_o^2}{\beta_o^2 (\gamma_o - 1)} \left[\frac{1}{A^2 (1 - A)^2} - \frac{3}{A (1 - A)} \right] dA \qquad (4)$$

Kar and Basu[7] have given a relativistic treatment of the scattering, basing their work on the Klein-Gordon equation. Neglecting "critical approach" their expression for the scattering cross section is identical to that of Møller without the spin term, i.e. relativistic Mott. For the primary energies of the present experiment, the deviation of the Kar and Basu cross section from the relativistic Mott cross section is less than one percent. For small A, Equations (2), (3) and (4) reduce to the classical expression of Bohr[4]:

$$\sigma(T)dT = \frac{2\pi e^4}{m v_o^2} \frac{dT}{T^2} \qquad (5)$$

where T is the kinetic energy of the knock-on electron.

Experimentally, the scattering problem has been studied by several investigators[8-20]. A resumé of the experimental work may be found in the paper of Groetzinger et al.[17]. With the exception of the study of Scott et al.[19], none of these experiments were of sufficient precision to discriminate between Mott and Møller scattering.

Scott, et al. succeeded in extracting the beam of the Illinois betatron which afforded them 15.7 Mev electron primaries. By counting the magnetically analyzed secondary electrons, scattered from various settings of foils in a scattering chamber, they were able to discriminate between Mott and Møller scattering and found a clear-cut preference for the latter.

From the literature one may conclude the following: (1) for collisions of small A, Bohr's classical theory in some regions of energy has been verified; (2) for collisions of large A, Mott scattering is preferred over classical theory in the non-relativistic limit (Møller's cross section reduces to the Mott expression as $\gamma \longrightarrow 1$); in the relativistic limit (up to 15.7 Mev) Møller's cross section gives an adequate relativistic description of the scattering and is definitely perferred to either the relativistic Mott or the Bohr scattering. Apparently, the observed scattering in the relativistic limit is described by either the Møller or relativistic Rutherford expression. The closeness of these two expressions as $\gamma \longrightarrow \infty$ arises from the near cancellation of the exchange term by the spin term in the Møller expression, Eq. (1).

2. Positron-Electron Scattering

Positron-electron scattering differs from electron-electron scattering not only in the fact that the secondary or scattered particles are now distinguishable, but also in exchange effects. Bhabha[21] has calculated the probability of a moving positron imparting a kinetic energy, T, to an electron initially at rest (laboratory system).

The differential scattering cross section of Bhabha in terms of A, defined as the ratio of T to the kinetic energy of the initial position in the laboratory system is:

$$\sigma(A)dA = 2\pi r_o^2 \frac{\gamma_o}{(\gamma_o - 1)^2 A^2} F(\gamma_o, A)\, dA \qquad (6)$$

where

$$F(\gamma_o, A) = \frac{1}{\gamma_o(\gamma_o+1)}\left[\left\{1 + 2(\gamma_o - 1)(1 - A) + (\gamma_o - 1)^2\left(1 - A + \frac{1}{2}A^2\right)\right\}\right.$$
$$+ \frac{(\gamma_o - 1)^2}{(\gamma_o + 1)^2} A^2\left\{3 + 2(\gamma_o - 1) + (\gamma_o - 1)^2\left(\frac{1}{2} - A + A^2\right)\right\}$$
$$\left. - \frac{(\gamma_o - 1)}{(\gamma_o + 1)} A\left\{3 + 4(\gamma_o - 1)(1 - A) + (\gamma_o - 1)^2(1 - A)^2\right\}\right]$$

where r_o is the classical electron radius, $\gamma_o = \left(1 - \left(\frac{v_o}{c}\right)^2\right)^{-1/2}$, and v_o is the initial velocity of the positron in the laboratory system. According to Bhabha, the first term in the square brackets of $F(\gamma_o, A)$, is the ordinary scattering. The second term represents the contribution of exchange. The third term results from the interference between the ordinary scattering and the latter process. Equation (6) reduces to the classical Bohr theory, Equation (5), for small A.

Several experiments have been performed to detect Bhabha's exchange effect[22-27]. Until the recent work of Howe and MacKenzie[27], none of the experiments were of sufficient accuracy to demonstrate the presence of exchange. The results of the latter experiment definitely support the inclusion of Bhabha's exchange term. Positron-electron scattering for $A < 0.1$ has not been studied prior to the present work.

For the primary energies of the present study, Equation (2), to a sufficient approximation, may be written:

$$\sigma(A)dA = \frac{2\pi r_o^2}{\gamma_o}\left[\frac{1}{A(1 - A)} - 1\right]^2 \qquad (7)$$

Similarly, Equation (6) may be written:

$$\sigma(A)dA = \frac{2\pi r_o^2}{\gamma_o A^2}\left[1 - A(1 - A)\right]^2 dA \qquad (8)$$

In emulsion the scattered positron and electron are indistinguishable. Therefore, the observable cross section in emulsion, $\sigma_o(A)$, is the sum:

$$\sigma_o(A) = \sigma(A) + \sigma(1 - A) \quad 0 \leq A \leq 0.5$$

Equation (8) then becomes:

$$\sigma_o(A)dA = \frac{2\pi r_o^2}{\gamma_o}\left[1 - A(1 - A)\right]^2\left[\frac{1}{A^2} + \frac{1}{(1 - A)^2}\right]dA \qquad (9)$$

If the exchange terms in Equation (6) are omitted, the observable cross section, $\sigma_o'(A)$, is:

$$\sigma_o'(A)dA = \frac{2\pi r_o^2}{\gamma_o}\left[1 + \frac{A}{(1 - A)^2} + \frac{1 - A}{A^2}\right]dA \qquad (10)$$

The expressions (9) and (10) are symmetrical in A and (1 - A) as in the case of electron-electron scattering. For ~174 Mev primaries, the expected number of scattering events in emulsion from A = 0.1 to A = 0.5 (Figure 7) is about one per 100 cm of track. For this region of A, the cross section at this energy is practically unobservable in emulsion. At a primary energy of ~39 Mev, however, the expected mean free path for the same region of A is about 20 cm. Therefore, the study of the scattering in the region, $0.2 \leq A \leq 0.5$, has been carried out at this primary energy.

B. Method of Analysis

1. Scanning Procedure

The plates exposed to 200 Mev and 40 Mev (Fig. 1) electrons and positrons were scanned under ~500 x magnification. Ranges and angles were measured under ~1500 x and ~1000 x magnification, respectively. The length of primary track scanned was measured with the microscope stage coordinates. Tracks were not scanned and no event was recorded within 10 microns of either surface of the emulsion. Primary tracks were not scanned beyond a detectable nuclear scatter or electron-electron or positron-electron scatter of large A. The average track length in emulsion was about 0.4 cm for the 200 Mev exposures and 0.2 cm for the 40 Mev exposures. The mean energies of primary particles in emulsion were determined by measuring their multiple scattering over an average track length, (Appendix III). The scattering factors[28] used were K = 26.4 Mev degs/$(100\ \mu)^{1/2}$ for the 200 Mev exposures and K = 23.6 Mev deg/$(100\ \mu)^{1/2}$ for the 40 Mev

exposures. The mean primary energies determined from these measurements and the standard deviations of the energy spreads about the means are given together with the calculated losses in Appendix IV.

2. Measurements

The differential cross sections for electron-electron and positron-electron scattering are to be measured in terms of the energy of the knock-on electron. This may be determined by measuring either the range in emulsion or the angle of scatter.

Knowledge of the shrinkage factor of the emulsion is necessary in order to reconstruct the ranges and angles associated with scattering events (Appendix V). This was determined by passing 340 Mev alpha-particles through the undeveloped emulsion at an angle of 45° to the emulsion surface[29] and then measuring the ratio of the horizontal to the verticle projection after development. This ratio gave the shrinkage factor directly as 2.5 ± 0.1.

For each scattering event, both the range and angle of scatter were measured whenever possible. For very small energies, the angle was ill-defined because of multiple scattering. In this case, however, the energy may be determined from the range. For energies greater than 0.6 Mev nearly all knock-on electrons left the emulsion, but the angle of scatter could now be accurately measured. The kinetic energy of the scattered electron, T, is related to the angle of scatter, θ, and the incident energy, T_o, by (Appendix VI):

$$T = \frac{T_o \cos^2 \theta}{1 + \frac{T_o}{2\,mc^2} \sin^2 \theta} \qquad (11)$$

where mc^2 is the rest energy of the electron. For $T_o \sin^2 \theta/2\, mc^2 \gg 1$, T, as determined by θ, is nearly independent of the primary energy. This condition is met by all observed events and so the variation in primary energy caused by losses in emulsion has been disregarded.

3. Corrections

a) Scanning Efficiency

The scanning efficiency of an observer was determined from the data of two observers who scanned independently the same primary

tracks. If N_o is the true number of events, observers 1 and 2 will record $\varepsilon_1 N_o$ and $\varepsilon_2 N_o$ events respectively, where ε_1 and ε_2 are their efficiencies. After the first observer records N_1 ($=\varepsilon_1 N_o$) events the second observer will contribute a number n ($= N_o \varepsilon_2 (1 - \varepsilon_1)$) events. The scanning efficiencies calculated from the relationship $\varepsilon_i = \frac{N_i}{N_i + n}$, ($i = 1, 2$) were found for two observers to be 0.90 ± 0.09 and 0.85 ± 0.08. The efficiency correction for the doubly scanned data was therefore taken to be 1.5 percent. The best estimate of the scanning efficiency for a third observer whose efficiency was not measured was taken to be 0.875 with a probable error of 10 percent. The efficiency correction for singly scanned was therefore 14.3 percent. The probable error of 10 percent was compounded with the statistical error for these data.

b) Resolution

Electron range-straggling along with errors in range and angle measurements introduce limitations in the energy definition of scattered electrons. The range-straggling for electrons is computed in Appendix VII. The corrections due to these effects are treated in Appendix VIII.

C. Experimental Results

Figure 8 is a plot of the range and energy (determined from the angle of scatter) of knock-on electrons produced from positron-electron* and electron-electron collisions in emulsion. The primary energy was 185 ± 37 Mev and 164 ± 21 Mev, respectively. These data were obtained from events in which both range and angle measurements were possible. All events had a projected angle of scatter less than 70^o. Zajac and Ross[30] measured the ranges of electrons of discrete energies up to 250 Kev in Kodak NT4 emulsion. Their results may

---

* For a given positron-electron collision, there is a finite probability that the scattered particle of lower energy is a positron rather than an electron. This probability in terms of A is: $P(A) = (\frac{A}{1 - A})^2 / 1 + (\frac{A}{1 - A})^2$, assuming $\sigma(A) \propto 1/A^2$. For the values of A in Figure 8, $P < 10^{-5}$. To a good approximation, therefore, the data of Figure 8 apply to knock-on electrons.

be fitted to the curve[31]:

$$R(\text{microns}) = 0.3\ T^{1.6}_{(\text{Kev})} \qquad (12)$$

where R is the mean range. Assuming a law of this form, a mean range was determined from the present data. The standard error of the mean range was found to be 6 percent (Appendix IX). This mean range and mean range of Zajac and Ross are plotted in Figure 8. The two curves differ by $\sim$ 7 percent.

The spread of the data may be attributed to: (1) range straggling, (2) errors in angle and range measurements, and (3) inelastic collisions. The effect of inelastic collisions is expected to be greater for positron-electron collisions than for electron-electron collisions[32]. If this effect is detectable, it would be manifested in a difference in spread of the two sets of points in Figure 8. It is found (Appendix IX) that the spread of both sets of data is adequately accounted for in terms of (1) and (2) above. Therefore, no inelastic scattering is observed for $A < 0.03$ within an accuracy of 5 percent.

Figures 9 and 10 are graphical representations of the electron-electron and positron-electron scattering results tabulated in Tables II and III. The data associated with 164 ± 21 Mev primary electrons and 185 ± 37 primary positrons are given in terms of T. The events initiated by 36.1 ± 3.6 Mev electrons and 42.9 ± 4.3 Mev positrons are analyzed in terms of A. The validity of the range-energy curve of Zajac and Ross for Ilford G-5 emulsions has been investigated by Bonetti and Tomasini[31]. From range measurements of monochromatic electrons between 80 and 150 Kev these authors found their values to be in good agreement with those of Zajac and Ross. This relationship (Eq. 12) is therefore used to analyze the present data between knock-on energies of 0.03 Mev to 0.40 Mev. Knock-ons with energies less than 0.03 Mev were not considered because of their small range ($<$ 7 microns) and the effects of electron binding.

The selection criterion for the remaining events, including those initiated by $\sim$39 Mev primaries, was the scattering angle. The data for $T > 0.1$ Mev has been obtained by the independent observations

of two scanners using the same ~174 Mev primary tracks. The remaining data, including those obtained from ~39 Mev primaries, were obtained by one observer. The probable error for a given interval $(\Delta x)_i$ (x = T or A) is placed at that abscissa, x_i, where the ordinate of the histogram equals the ordinate of the absolute theoretical cross section if the areas under the two are equal, i.e. x_i is the solution of $\sigma(x_i) = \int_{(\Delta x)_i} \sigma(x)\, dx/(\Delta x)_i$. The x_i's were computed in the case of electron-electron scattering from Møller's cross section (Equation 7) and for positron-electron scattering, from Bhabha's cross section including exchange (Equation 9). For perfect agreement with theory the experimental points should therefore be superimposed on these theoretical curves.

From Figures 9 and 10, the experimental results for $A < 0.2$ are in good agreement with theory over seven orders of magnitude of cross section. In the region $0.2 < A < 0.5$, the present electron-electron scattering results favor Møller scattering over that of Rutherford, Bohr, Mott or Kar and Basu. The present positron-electron scattering results are in agreement with Bhabha's theory for $0.2 < A < 0.5$. The statistical error is too great to distinguish between the Bohr and Bhabha cross section or to detect the presence of exchange. The experimental ratio of electron-electron scattering to positron-electron scattering in this region of A is 2.6 ± 1.3. This ratio given by the various theories of Figures 9 and 10 ranges from 2.6 (Møller/σ_o) to 1.2 (Mott/Bohr).

In the region where the various theories represented in Figures 9 and 10 are indistinguishable, the theoretical cross section is nearly independent of the primary energy. This can be shown by writing Equation (5) as:

$$\sigma(T)\, dT = \frac{2\pi r_o^2}{\beta_o^2}\, mc^2\, \frac{dT}{T^2} \qquad (13)$$

For the primary energies of this study, $\beta_o \approx 1$, thus $\sigma(T)$ is insensitive to the primary energy.

The ratios of the observed integrated cross section to the integrated theoretical cross section are: 0.94 (electron-electron scattering) and 1.08 (positron-electron scattering). The probable error

in each case is 10 percent. For the doubly scanned data ($T > 0.1$, or $A > 5.3 \times 10^{-4}$) these ratios are 0.94 ± 0.06 and 0.87 ± 0.04, respectively. The probable errors have been compounded from the statistical errors and the errors quoted by Zajac and Ross in their determination of the range-energy relationship. The fact that these ratios are less than unity is probably due to a small systematic error in determining the scanning efficiency of an observer. If there is a correlation between missed events for two observers, their efficiencies determined by double scanning will be nearer unity than their true efficiencies. It is reasonable to suspect that such a correlation exists for knock-on electrons leaving the primary track in the plane perpendicular to the focal plane of the microscope.

The number of electrons per cubic centimeter of emulsion was calculated to be 1.07×10^{24} from the emulsion composition given by Ilford Ltd. The effect of water absorbed in the emulsion from the atmosphere on the electron density has been measured and is negligible in this experiment.

IV THE RATIO OF PLATEAU TO MINIMUM GRAIN DENSITY FOR ELECTRONS

A. Exposure and Method of Analysis

A single 1 inch x 3 inch, 200 micron Ilford G-5 emulsion was exposed to 300 Mev electrons and to 3 Mev electrons. The plate was exposed so that the primary electrons entered the emulsion perpendicularly to the leading edge and at an angle of $\sim 5^{\circ}$ to the emulsion surface. 3 Mev electrons emerging from the evacuated channel (Figure 3) and 300 Mev electrons arriving from the converter (Figure 1) penetrated the emulsion in opposite directions and formed two adjacent bands of electron tracks.

Grain counts were recorded in terms of a standard reticule unit, which, under the magnification used ($\sim$2500 x), was 32 microns in length. For the purposes of comparing grain counts at the two energies, the following criteria were adopted:

1. A grain was counted as one unit regardless of size.
2. All grain counts were taken in a layer of developed emulsion between 40 and 10 microns from the emulsion-air surface.
3. Track sections were accepted for grain counting only if their dip angle was in the same sense as would be expected from the exposure set up.
4. Consistent with (3), only portions of track were grain counted where the angle of dip in the developed emulsion was between 0 and arc tan 0.059.

The grain density determined on the basis of criterion (1) is essentially proportional to that obtained when clumps are resolved into individual grains for the thin tracks used here. The fourth criterion allows one to neglect the error in track length due to the uncertainty in the shrinkage factor. By grain counting $\sim$ 300 Mev electron tracks as they penetrated the emulsion the gradient of development in the acceptable layer (criterion 2) was found to be less than one percent. Because of the large multiple scattering of $\sim$ 3 Mev electrons, and in light of criterion (4) it was not feasible to grain count successive intervals

of given tracks. Instead, the following "field of view" method was adopted: grain counts per standard unit were taken for all portions of ~ 3 Mev tracks in a field of view lying within ± 22.5 degrees of the mean entrance angle. Electron tracks of ~ 300 Mev were first grain counted by taking successive intervals of given tracks (7207 grains). Then ~ 3 Mev electron tracks were grain counted by the "field of view" method (7002 grains). Finally, ~ 300 Mev electron tracks were grain counted by the latter method (7097) grains). The means and standard deviations of the grain density distributions of the two sets of ~ 300 Mev data agreed within the statistical errors. The error in track length due to multiple scattering over a standard unit is negligible. All counts were taken by one observer whose reproducibility was found to be better than one percent.

B. Experimental Results and Theory

The relativistic rise in ionization of a charged particle moving through matter has been a subject of considerable interest from both the experimental[33-42] and theoretical[6, 43-53] view points. Contributions to the experimental investigations of this phenomenon from nuclear emulsion studies usually consist of combining grain counts of tracks produced by charged particles moving in emulsion with multiple scattering measurements. Thus, the relationship of the grain density, g, as a function of velocity, e.g. γ, is determined. Knowledge of g as a function of $|dT/dx|$ allows one to find the desired relationship between $|dT/dx|$ and γ.

The fact that the ionization saturates at large values of γ is well established[34, 40]. Measurements of the magnitude of this saturation value with respect to minimum ionization has in some cases led to conflicting results. Practically all investigations in nuclear emulsions have led to a comparison of the saturation ionization for electrons and mesons to minimum ionization of mesons. Although $|dT/dx|$ is presumed to be independent of the mass, it is preferable for a precise determination of this effect to utilize particles of the same mass.

The results of the grain counts of 2.8 Mev and 293 Mev electrons are shown in Figure 11. The equivalence of the "field of view"

and "successive interval" methods of grain counting is demonstrated by comparing the grain density distributions of 293 Mev electrons for both cases. The mean energies of 2.8 Mev and 293 Mev have been calculated[52] from the energy loss due to ionization and radiation in the acceptable layer of emulsion for electrons entering the emulsion at 3 Mev and 300 Mev, respectively. Both energies are located at essentially flat portions of the specific ionization curve. A calculation using the constants for emulsion given by Sternheimer[52] shows that the ionization of 2.8 Mev electrons differs from the minimum ionization by less than one percent. The ratio of the mean grain densities of 293 Mev and 2.8 Mev tracks is: $g_{293}/g_{2.8\ \mathrm{Mev}} = 1.087 \pm 0.010$. The standard error is computed from the standard deviations of the grain density distributions for the two energies. A statistical test[54] of the compatibility of the two standard deviations, taking into account the difference in the means, shows that the probability that they are equal is approximately 95 percent.

Assuming the law of proportionality between g and $|dT/dx|$[35], the results of the present study show that the specific ionization for electrons saturates at a value 8.7 ± 1.0 percent above minimum ionization. This value is in good agreement with the results of McDiarmid[39], Morrish[40], and Voyvodic[37]. These authors give the ratios: $\frac{g_{40\ \mathrm{Mev}}}{g_{3.5\ \mathrm{Mev}}} \sim$ 7 percent, $\frac{g_{\mathrm{plateau}}}{g_{9\ \mathrm{Mev}}} \sim 5$ percent and $\frac{g_{\mathrm{plateau}}}{g_{\mathrm{min.}}} \sim 8$-9 percent, respectively. Stiller and Shapiro* in a study of the grain densities of mesons and electrons report an increase of 14 ± 3 percent beyond minimum which is significantly higher than the present results.

The observed increase in grain density can be explained from the theory of Fermi[46] extended by Wick[47], Halpern and Hall[48], A. Bohr[49], Schönberg[51] and Sternheimer[52], or from the theory of Huybrechts and Schönberg[53]. In the former theory, the increase in $|dT/dx|$ at relativistic energies arises from the emission of Cerenkov radiation. An increase in grain density due to this mechanism would therefore demand strong absorption of the high energy Cerenkov radiation in silver halide crystals. In an alternative treatment, Huybrechts and

---

* Private Communication.

Schönberg[53] proposed a modification of Fermi's methods which reduces the intensity of the high energy Cerenkov bands and gives a larger amount of ionization.

For a cut-off energy for delta-ray production taken at 5 Kev the theory developed along Fermi's methods predicts an increase in $|dT/dx|$ of eleven percent[52]. Assuming proportionality between g and $|dT/dx|$ the present results indicate that about four-fifths of the Cerenkov radiation goes into producing counted grains. For the same cut-off, the theory of Huybrechts and Schönberg predicts an increase in $|dT/dx|$ of 3.8 percent. These authors point out, however, that small energy transfers are probably not sufficient to render an Ag Br grain developable. By neglecting the contribution of the electrons of the outer shell and thirty-three percent of the contribution of the next shell, the increase from minimum to saturation becomes 6 percent. Thus, with suitable modifications, this theory also explains the present experimental results.

V THE NUCLEAR SCATTERING OF ELECTRONS AND POSITRONS

A. Method of Analysis

The scanning procedure here is essentially that described in Chap. III B 1. To circumvent errors in the determination of the scattering angle due to the uncertainty in the shrinkage factor, angles of scatter were recorded in terms of their projected angles. These measurements were made to 0.5 degree with the aid of a goniometer affixed to an eye piece of the microscope. All scatters which had a projected angle greater than 3 1/2 degrees (Fig. 12) were recorded. This is larger than the mean scattering angle by a factor ~ 5. The observer resolution was determined by the remeasurement of angles. This was compounded with the expected multiple scattering over the reticule length used in angle measurements to give the total resolution function. For small angles the expected scattering is given by the Rutherford cross section which in terms of the projected angle δ varies as $1/\delta^3$. From a treatment similar to that of Appendix VIII one finds that the resolution correction corresponding to the angle δ is $(1 + 6\frac{\sigma_\delta^2}{2} + \cdots)$ where σ_δ is the standard deviation of the resolution function. The largest scattering angle observed had a projected angle of 87 degrees (electron-nuclear scatter).

B. Experimental Results and Comparison with Theory

A convenient method of comparing the present results with theory is to first fold the theoretical cross section into the plane of the projected angle. The scattering law of Rutherford,

$$\sigma(\theta) = A \csc^4 \frac{\theta}{2} \tag{14}$$

where $A = \left(\frac{Z c^2}{2 m c^2}\right)^2 \frac{(1 - \beta_o^2)}{\beta_o^4}$, and θ is the scattering angle, is an obvious choice to describe in the first approximation the observed scattering. This law in terms of the projected angle, δ, is (Appendix X)

$$W(|\delta|)\, d\delta = \frac{16 A\, d\delta}{\sin^2 \delta} \left[1 + (\pi - |\delta|) \operatorname{ctn} |\delta|\right] \tag{15}$$

where $W(|\delta|)\, d\delta$ is the probability of a scatter between $|\delta|$ and $|\delta| + d|\delta|$. Because of the additive property of the scattering cross section the observed scattering in a mixture of elements, viz. emulsion, is the sum of the individual cross sections. Thus, Equation (15) is more conveniently written in terms of $\ell(|\delta|)$, the mean free path for scattering between $|\delta|$ and $|\delta| + d|\delta|$:

$$\frac{d\delta}{\ell(|\delta|)} = \sum_i N_i Z_i^2 r_o^2 \frac{(1 - \beta_o^2)}{\beta_o^4} \frac{4\, d\delta}{\sin^2 \delta} \left[1 + (\pi - |\delta|) \operatorname{ctn} |\delta|\right]$$

The summation is calculated from the emulsion composition to be 37.0×10^{24} cm^{-3}. This corresponds to a root mean square Z for emulsion of 21.4.

The results of the nuclear scattering of 36.1 ± 3.6 Mev electrons and 42.9 ± 4.3 Mev positrons are tabulated in Table IV and plotted in Figure 13.

In the small angle approximation, the Rutherford cross section (Eq. 14) has the following properties: (1) the integrated cross section $\int_\theta^\pi \sigma(\theta)\, d\Omega$, and $\int_\delta^\pi W(|\delta|)\, d\delta$ are equal if $\theta = \delta$, and (2) the probabilities of scattering into the interval $\Delta\delta$, and into the element of solid angle $d\Omega(\theta)$ $(= 2\pi \sin\theta\, \Delta\theta)$ are equal, if $\theta = \delta$ and $\Delta\theta = \Delta\delta$ (Appendix XI). This approximation is found to be valid for the angular intervals of the histograms of Fig. 13. It follows that the angles plotted along the abscissa may be interpreted either as δ or θ.

In theoretical treatments of the multiple scattering of charged particles the effects of the finite size of the nucleus and the possibility of forces other than electromagnetic are usually assumed smaller than the coulomb interaction[55, 56, 57]. This has not been tested in the photographic plate for high energies[58]. The results of the present investigation show that the non-Gaussian tail to the multiple scattering distribution for electrons and positrons is described by the Rutherford law (Eq. 14) for energies ~ 39 Mev.

VI POSITRON ANNIHILATION IN FLIGHT

The annihilation of fast positrons in matter has recently been investigated by Colgate and Gilbert* [59]. The observed cross section in Be and Li H was found to be in agreement with the two-quantum annihilation cross section given by Dirac. Bramson, et al. [60] in a study of decay positrons emitted by μ mesons in G-5 emulsions report an annihilation length in emulsion consistent with Dirac's theory [61].

For each annihilation observed in the present work (Fig. 14) the track was extrapolated beyond the point of annihilation by maintaining the projected angle and dip angle. This was done to determine whether (1) the track reappeared, or (2) a pair was initiated by the forward moving photon. In no case were these observed.

From the calculated pair production length in emulsion [62] (assuming the forward moving photon carries off the positron energy [63]) and the extrapolated distance in emulsion, the probability that a pair will be produced is 0.03. For each event the multiple scattering of the positron track was measured up to the point of annihilation. The energies determined in this way were consistent with the mean energies of Appendix IV.

The annihilation events are analyzed in Table V and compared with the two-quantum annihilation cross section of Dirac. The cross section in G-5 emulsion for annihilation in flight is seen to be of the same order of magnitude as that given by theory. The contribution to the cross section due to one or zero quantum annihilation processes is negligible here [64].

---

* This experiment was undertaken in part to further investigate the disappearance of fast electrons in emulsion reported by W. Barkas, R. Deutsch, F. Gilbert and C. Violet, Phys. Rev. 86, 59 (1952). Further study revealed that these events are correctly interpreted as the annihilation in flight of positrons (Erratum Phys. Rev. 88, 1435 (1952)). The results of Colgate and Gilbert also confirm this interpretation.

VII PAIR PRODUCTION

The direct pair production by a charged particle moving through matter has been a subject of considerable experimental investigation[18, 65-75]. This phenomenon has for the most part eluded observation and was only recently directly observed in photographic emulsions[18, 71, 73, 74]. Since the direct pair production cross section is little known from experiment we include here an analysis of the pairs observed in the present study.

A charged particle penetrating matter initiates a pair either in the field of a nucleus or an electron. Elementary considerations show that the probability of the latter process is of the order of $\frac{1}{Z}$ ($\approx \frac{1}{13}$ for emulsion) times that of the former. In G-5 nuclear emulsions the two processes can be distinguished by observing the recoil electron in the latter case. According to Bhabha[76], the cross section for direct pair production in the field of a bare nucleus is:

$$\frac{28}{27\pi}\left(\frac{Z}{137}\right)^2 r_o^2 \left[\ell n\,(a\,\gamma)\right]^3$$

where a is a constant of the order of unity.

In Table VI the three events observed in the present study (Fig. 15) are analyzed and compared with the theory of Bhabha, using the experimentally determined value of a[75]. The experimental values are consistent with Bhabha's theory. No events were observed in which a pair was initiated in the field of an electron. The track lengths in Table VI are therefore lower limits to the mean free paths for this process.

VIII SUMMARY

These investigations into the processes enumerated in the Introduction has yielded the following results:

1. Electron-Electron Scattering

The measured differential scattering cross section for small A is in good agreement with theory (Bohr) over seven orders of magnitude of the cross section. For large A, the observed scattering tends to discriminate in favor of Møller's cross section as opposed to those of Rutherford, Bohr, and Kar and Basu.

2. Positron-Electron Scattering

For small A the experimental results here are in essential agreement with the electron-electron scattering results over the same range of A and cross section. Because of the indistinguishability of scattered electrons and positrons in emulsion the present method is not sensitive to distinguishing between the Bohr and Bhabha (with and without exchange) cross sections at large A. The present results, however, are in general agreement with the Bohr and Bhabha theories in the region of large A.

3. Ionization Losses

The ratio of plateau grain density to minimum grain density for electrons in Ilford G-5 emulsion has been determined to be 1.087 ± 0.010. From Fowler's investigations, this ratio may be interpreted as that of saturation ionization to minimum ionization. This increase may be satisfactorily accounted for in terms of the theory developed along Fermi methods or the theory of Huybrechts and Schönberg.

4. Nuclear Scattering of Electrons and Positrons

The results obtained from the nuclear scattering of $\sim$39 Mev electrons and positrons show that the non-Gaussian tail to the multiple scattering distribution in Ilford G-5 emulsion is described in terms of the Rutherford scattering cross section.

5. Positron Annihilation in Flight

The observed annihilation length at energies of 185 ± 37 and 42.9 ± 4.3 Mev in Ilford G-5 emulsion agrees in order of magnitude with the two-quantum annihilation cross section of Dirac.

6. Pair Production

The pair production length in Ilford G-5 emulsion was found to agree in order of magnitude with Bhabha's cross section for the primary energies of 164 ± 21 Mev and 288 Mev.

7. Inelastic Electron-Electron and Positron-Electron Collisions

For $A < 0.03$ no inelastic scattering was observed within an accuracy of five percent.

Acknowledgments

I am indebted to Dr. W. H. Barkas for first suggesting this study to me and for many enlightening discussions concerning the experimental and theoretical aspects of this investigation.

The assistance of Mr. F. C. Gilbert and Mr. R. W. Deutsch in exposing the plates and in much of the scanning as well as their many helpful comments is gratefully acknowledged.

The grain counts of Mr. R. P. Michaelis have been an invaluable contribution to the present work.

I am grateful to Mrs. Jennie Louie for her assistance in the multiple scattering and nuclear scattering measurements.

Much of the microscope work of the preliminary phases of the present study was done by Professor Lawrence Germain and Mrs. Edith Goodwin to whom I owe a debt of gratitude.

I am indebted to Mr. Al Oliver for his microphotographs and helpful advice on processing emulsions.

The assistance of Mr. Phillip Carnahan in the processing of emulsions by the "Bristol method" is gratefully acknowledged.

I am grateful to Dr. R. S. White and Mr. J. W. McLeod for their assistance in the electron linear accelerator exposures as well as Professor A. C. Helmholz, Mr. George McFarland and members of the synchrotron operating crew for their cooperation in the synchrotron exposures.

This work was assisted by the continued interest and support given the film program by Professor R. L. Thornton and Professor E. O. Lawrence.

APPENDIX I

Development Procedure[2]

Pre-Soak (distilled water, room temperature)	1 hour
Cold Developer* (5° C.)	1 hour
Hot Developer* (26° C.)	30 minutes
Cold Soak (5° C.)	1 hour
Fixing** (room temperature, with agitation)	6 hours
Washing (room temperature)	24 hours
Drying	24 hours

*Amidol Developer

Distilled Water	1000 cc.
Boric Acid	35 gm.
Sodium Sulfite (anhydrous)	18 gm.
Potassium Bromide (10 percent solution)	8 cc.
Amidol (Acrol)	4.5 gm.

**Kodak Acid Fixer

APPENDIX II

Development Procedure[3]

Soak in distilled water	25 mins.
Developer* (5° C.)	15 mins.
"Hot Plate" (27° C.)	25 mins.
Stop bath (5° C.)	10 mins.
Fixing** (room temperature)	2 hrs.
Washing	4 hrs.
Drying	6 hrs.

*Developer

Amidol	3.0 gs
Anhydrous sodium sulphite	6.7 gs
Sodium bisulphite liquor (S.G. 1.34)	1.4 mls
Distilled water (add)	930 mls

**Fixer

Sodium thiosulphate	400 gs
Sodium bisulphite	30 gs
Water to add	1000 mls

APPENDIX III

Calculation of the Mean Primary Energy in Emulsion and the Spread of Primary Energies about the Mean from Multiple Scattering Measurements

Let: $p(\delta, T)$ be the probability that a particle of energy T be scattered between the angles δ and $\delta + d\delta$ per cell length.

$q(\delta - \delta_o)$ be the probability that an angle δ be observed between δ_o and $\delta_o + d\delta_o$ per cell length.

$r(\langle T \rangle - T)$ be the probability that the particle has an energy between T and T + dT.

For a given T, the second moment of the observed angle is:

$$\begin{aligned}\langle \delta_o^2 \rangle_T &= \iint \delta_o^2 \, p(\delta, T)\, q(\delta - \delta_o)\, d\delta \, d\delta_o \\ &= \iint \left[(\delta - \delta_o)^2 + 2\,\delta\,\delta_o - \delta^2 \right] p(\delta, T)\, q(\delta - \delta_o)\, d\delta \, d\delta_o \qquad (16) \\ &= \langle \delta^2 \rangle + \langle \delta_\varepsilon^2 \rangle\end{aligned}$$

$\langle \delta_\varepsilon^2 \rangle$ is the second moment of the resolution function $q(\delta - \delta_o)$ and is computed from the relationship: $\langle \delta_\varepsilon^2 \rangle = \langle \delta_n^2 \rangle + \langle \delta_R^2 \rangle$ where δ_n is the stage noise and δ_R is the observer error. Since $\langle \delta_\varepsilon^2 \rangle$ is small compared to $\langle \delta^2 \rangle$, Equation 15 may be written:

$$\langle |\delta_o| \rangle_T = \langle |\delta| \rangle \left(1 + \frac{1}{2} \frac{\langle |\delta_\varepsilon| \rangle^2}{\langle |\delta| \rangle^2} - \frac{1}{8} \frac{\langle |\delta_\varepsilon| \rangle^4}{\langle |\delta| \rangle^4} + \cdots\cdots\right) \qquad (17)$$

assuming δ_o, δ, and δ_ε to be normally distributed. To consider the effect of a spread in primary energy we write Equation 17 as:

$$\langle |\delta_o| \rangle_T = \frac{K}{T} + \frac{\langle |\delta_\varepsilon| \rangle^2}{2} \frac{T}{K} - \frac{\langle |\delta_\varepsilon| \rangle^4}{8} \frac{T^3}{K^3} \cdots\cdots$$

where K is the scattering factor, and compute the integral

$$\langle|\delta_o|\rangle = \int \langle|\delta_o|\rangle_T \, r(\langle T\rangle - T)\, dT$$

$$= \frac{K}{\langle T\rangle}(1 + \beta_2 + \beta_4 + \cdots) + \frac{\langle|\delta_\varepsilon|\rangle^2}{2}\frac{\langle T\rangle}{K} + \text{4th and higher order terms} \qquad (18)$$

assuming $r(\langle T\rangle - T)$ is symmetrical. β_i is the i^{th} moment of $(\frac{\langle T\rangle - T}{\langle T\rangle})$. Assuming $r(\langle T\rangle - T)$ is also normally distributed, Equation 18 becomes, in terms of μ, the fractional standard deviation in energy:

$$\langle|\delta_o|\rangle = \frac{K}{\langle T\rangle}(1 + \mu^2) - \frac{\langle|\delta_\varepsilon|\rangle^2}{2}\frac{\langle T\rangle}{K} \qquad (19)$$

to third order in μ.

From these same considerations one calculates:

$$\langle\delta_o^2\rangle = \langle\delta_\varepsilon^2\rangle + \frac{\pi}{2}\frac{K^2}{\langle T^2\rangle}(1 + 3\mu^2) \qquad (20)$$

th third order in μ.

From the condition that $\mu^2 > 0$ the upper limits of $\langle|\delta_\varepsilon|\rangle$ and $\langle\delta_\varepsilon^2\rangle$ can be calculated from Equations 19 and 20 for the detection of an energy spread about $\langle T\rangle$. Assuming that this condition is met, Equations 19 and 20 can be solved for the two unknown quantities μ and $\langle T\rangle$.

APPENDIX IV

Comparison of the Mean Primary Energies in Ilford G-5 Emulsion with the Calculated Values

The multiple scattering measurements give the following results:

Exposure	Mean Primary Energy (Mev) with probable error	Percent Standard Deviation of energy spread in emulsion
200 Mev electrons	164 ± 21	20 ± 16
200 Mev positrons	185 ± 37	10 ± 8
40 Mev electrons	36.1 ± 3.6	25 ± 20
40 Mev positrons	42.9 ± 4.3	17 ± 13

The ionization loss in Ilford G-5 emulsion for particle energies of 200 Mev and 40 Mev is calculated to be[52]:

$$\left|\frac{dT}{dx}\right| = 4.2 \text{ Mev/cm}$$

The energy loss by radiation can be computed from the expression: $T = T_o \exp - x/\ell$ where T_o is the initial energy, T is the energy after traveling a distance x in emulsion, and ℓ is the radiation length for emulsion. The radiation length is defined[77]:

$$\frac{1}{\ell} = N \frac{Z^2 r_o^2}{137} \left[4 \ln (183 Z^{-1/3}) + 2/9\right]$$

where N = number of nuclei per unit vol

Z = nuclear charge

r_o = classical electron radius

For emulsion we take for ℓ, the weighted average:

$$\frac{1}{\ell} = \frac{r_o^2}{137} N_o \sum_i Z_i^2 \left(4 \ln 183 Z_i^{-1/3} + \frac{2}{9}\right) \frac{g_i}{A_i}$$

where: N_o = Avogadro's number

Z_i = nuclear charge of the i^{th} element

g_i = density of the i^{th} element

A_i = atomic weight of the i^{th} element

Using the values given by Ilford Ltd. for the composition of G-5 emulsion, one calculates:

$\mathcal{l} = 2.90$ cm

This is in agreement with Corson's[78] value. From the above values of $|dT/dx|$, and $\mathcal{l}$, the mean energy in emulsion corresponding to the measured average track lengths are:

Exposure	Average Track Length	Mean Energy
200 Mev	0.4 cm	185 Mev
40 Mev	0.2 cm	38 Mev

APPENDIX V

The Measurement of Ranges and Angles

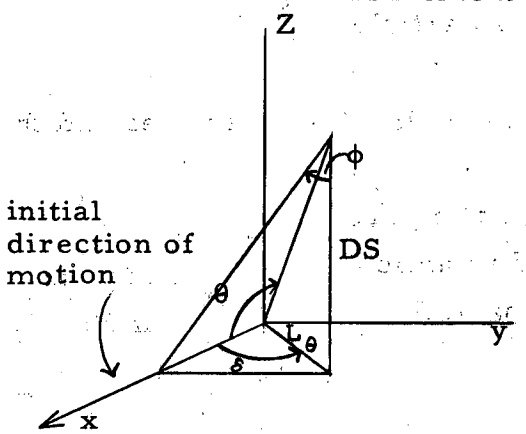

Fig. 16

θ = angle of scatter

δ = projected angle of scatter

D = depth measurement

S = shrinkage factor

L_θ = projection of scattered track corresponding to D for a given θ.

$a = \frac{DS}{L}$

The origin is the point of scatter. The xy plane is the focal plane of the microscope. To a good approximation, the initial direction of motion is the x axis.

In the analysis of events in emulsion one measures directly D, L_θ, and δ.

Range Measurements

The range of a highly scattered electron track is measured by dividing the track into convenient sections and measuring L_i and D_i for the i^{th} section. The range for a track of N sections is then:

$$R = \sum_{i=1}^{N} L_i (1 + a_i^2)^{1/2} \qquad (21)$$

Angle Measurements

From Figure 1 the relationship between θ, δ, and a is:

$$\cos\theta = \frac{\cos\delta}{\sqrt{1 + a^2}} \qquad (22)$$

APPENDIX VI

The Kinetics of the Elastic Collision of Two Equal Mass Particles

Let:

θ = the angle between the direction of scatter and the incident direction

T = the kinetic energy of a particle

P = the momentum of a particle

v = the velocity of a particle

$\beta = v/c$

$\gamma = 1/(1 - \beta^2)^{1/2}$

c = velocity of light

m = mass of the particles

Subscripts: o - refers to incident particle

1 - refers to lower energy secondary particle

2 - refers to higher energy secondary particle

Energy Conservation

$$T_o = T_1 + T_2$$

$$m(\gamma_o - 1)c^2 = m(\gamma_1 - 1)c^2 + m(\gamma_2 - 1)c^2$$

$$\gamma_o + 1 = \gamma_1 + \gamma_2 \qquad (23)$$

Momentum Conservation

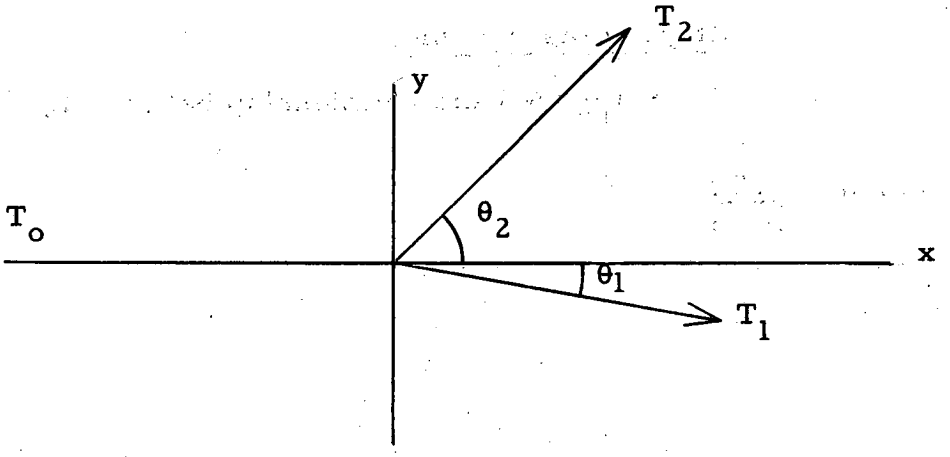

Fig. 17

$$\Sigma P_x = 0$$

$$m \beta_o \gamma_o c = m \beta_1 \gamma_1 c \cos \theta_1 + m \beta_2 \gamma_2 \cos \theta_2$$

since $\beta \gamma = \sqrt{\gamma^2 - 1}$

$$\sqrt{\gamma_o^2 - 1} = \sqrt{\gamma_1^2 - 1} \cos \theta_1 + \sqrt{\gamma_2^2 - 1} \cos \theta_2 \qquad (24)$$

$$\Sigma P_y = 0$$

$$m \beta_1 \gamma_1 c \sin \theta_1 = m \beta_2 \gamma_2 c \sin \theta_2$$

or

$$\sqrt{\gamma_1^2 - 1} \sin \theta_1 = \sqrt{\gamma_2^2 - 1} \sin \theta_2 \qquad (25)$$

eliminating θ_2 between Eq. 24 and Eq. 25:

$$(\gamma_2^2 - 1) = (\gamma_o^2 - 1) + (\gamma_1^2 - 1) - 2\sqrt{(\gamma_o^2 - 1)(\gamma_1^2 - 1)} \cos \theta_1 \qquad (26)$$

eliminating γ_2 between Eq. 23 and Eq. 26

$$\gamma_o \gamma_1 - \gamma_o + \gamma_1 - 1 = \sqrt{(\gamma_1^2 - 1)(\gamma_o^2 - 1)} \cos \theta_1$$

$$\cos^2 \theta_1 = \frac{(\gamma_o + 1)(\gamma_1 - 1)}{(\gamma_o - 1)(\gamma_1 + 1)}$$

or

$$T_1 = \frac{T_o \cos^2 \theta_1}{1 + \frac{T_o}{2 mc^2} \sin^2 \theta_1} \qquad (11)$$

For $\sin^2 0_1 \gg 2 mc^2/T_o$, Eq. 11 reduces to $T_1 = 2 mc^2 \cot^2 \theta_1$. By further algebraic manipulation it may also be shown that

$$\tan \theta_1 \tan \theta_2 = 2/\gamma_o + 1$$

and that $\tan(\theta_1 + \theta_2) = (1 + 2\,mc^2/T_o)(\tan\theta_1 + \tan\theta_2)$. Thus it can be seen, that for $\theta_1 < 90^o$ and $\theta_2 < 90^o$, that $(\theta_1 + \theta_2) < 90^o$ for $T_o > 0$. In the classical case for $T_o << 2\,mc^2$, $(\theta_1 + \theta_2)$ approaches 90^o for all θ_1 or $\theta_2 \leq 90^o$.

APPENDIX VII

Calculation of the Range Straggling of Electrons

The range straggling of a particle of unit charge is given by[79]:

$$\langle \Delta R^2 \rangle = \frac{1}{2} k \, \varepsilon \int_0^{T_o} dT \left(\frac{dT}{dx}\right)^{-3} \qquad (27)$$

In the particular case of electrons:

$$k = 2 \pi NZ \, r_o^2 \, (mc^2)^2$$

$$\varepsilon = 1$$

NZ = electronic density in the stopping material

r_o = classical electron radius

mc^2 = rest energy of the electron

The range-energy relationship for electrons in Ilford G-5 emulsion is[31]:

$$T = K R^n \qquad (28)$$

where: $K = 8.8$ kev/(microns)^n

$n = 0.63$

To calculate in the first approximation the range straggling of electrons we combine Equations (27) and (28) and obtain:

$$\langle \Delta R^2 \rangle = \frac{k}{2 n^2 K^2} \, \frac{R_o^{3-2n}}{3 - 2n}$$

where R_o is the range. Using the value: $\sum_i N_i Z_i = 1.07 \times 10^{24}$ cm^{-3} calculated from the emulsion composition, one computes the fractional standard deviation of the range straggling to be:

$$\mu_s = \sqrt{\frac{\langle R^2 \rangle}{R_o^2}} = \frac{0.36}{R_o^{13}}$$

For ranges of 50 and 400 microns, μ is 20 and 16 percent, respectively. The measurements of Zajac and Ross[30] are in fair agreement with these values.

APPENDIX VIII

Calculation of the Effect of the Energy Resolution Upon the Magnitude of the Absolute Cross Section for Electron-Electron Scattering and Positron-Electron Scattering

Let

μ = fractional standard deviation of the energy resolution

μ_s = fractional standard deviation of the range straggling

μ_o = fractional standard deviation of the observer error in range measurement

T = energy of the scattered electron

T' = energy of scatter at which the cross section is being measured

$w(T-T')$ = curve of the resolving power

(T) = theoretical cross section

$Q(T)$ = observed cross section

It follows that:

$$Q(T') = \int w(T-T')\, \sigma(T)\, dT \tag{29}$$

Assuming the errors in range and angle measurements and the range straggling are normally distributed, $w(T-T') = C \exp (T-T')^2/2T^2\mu^2$, where C is the normalizing constant. With the exception of the data obtained from $\sim$39 Mev primaries, the theoretical cross section, to a good approximation, is given by: (see Eq. 13)

$$\sigma(T) = 2\pi r_o^2\, mc^2/T^2 \tag{30}$$

Equation 29 then becomes:

$$Q(T') = 2\pi r_o^2\, mc^2 \int \frac{C \exp (T-T')^2/2T^2\mu^2}{T^2}\, dT$$

Let: $T - T' = x$

$$Q(T') = 2\pi r_o^2\, mc^2 \left(\frac{1}{T'}\right)^2 \int \frac{C \exp x^2/2T^2\mu^2}{\left(1 - \frac{x}{T'}\right)^2} = 2\pi r_o^2\, mc^2 \left(\frac{1}{T'}\right)^2$$

$$\int C \exp x^2/2T^2\mu^2 \left(1 - 2\frac{x}{T'} + 3\left(\frac{x}{T'}\right)^2 + \cdots\right)$$

$$= 2\pi r_o^2\, mc^2 \left(\frac{1}{T'}\right)^2 \left(1 + 3\mu^2 + \cdots\right)$$

Recalling Equation 30, the observed cross section becomes:

$$Q(T') = \sigma(T')\ (1 + 3\mu^2) \tag{31}$$

neglecting 4th and higher powers of μ. In the region where the approximation, Equation 30, is not valid, Equations (7) and (9), must be used.

For electron-electron scattering the observed cross section from Eq. 7 is:

$$Q(A') = \frac{2\pi r_o^2}{\gamma} \int C \exp (A - A')/2A^2\mu^2 \left(\frac{1}{A^2(1 - A)^2} - \frac{2}{A(1 - A)} + 1\right) dA$$

$$= \frac{2\pi r_o^2}{\gamma} \left[\frac{2A' + 1}{A'^2}\left(1 + 3\mu^2 - \frac{4A'\mu^2}{2A' + 1}\right) + \frac{3 - 2A'}{(1 - A')^2}\right.$$

$$\left(1 + \left(\frac{A'}{1 - A'}\right)^2 \left(\frac{5 - 2A'}{3 - 2A'}\right)\mu^2\right) - \frac{2}{A'}(1 + \mu^2) - \frac{2}{1 - A'}$$

$$\left.\left(1 + \left(\frac{A'}{1 - A'}\right)^2 \mu^2\right) + 1\right] \tag{32}$$

Treating Bhabha's expression, Equation (9), in the same way, the observed cross section is:

$$Q(A') = \frac{2\pi r_o^2}{\gamma} \left[\frac{1}{A^{12}}(1 + 3\mu^2) - \frac{2}{A'}(1 + \mu^2) + 2 + (1 - A')^2\left(1 + \left(\frac{A'}{1 - A'}\right)^2 \mu^2\right)\right.$$

$$+ \frac{1}{(1 - A')^2}\left(1 + 3\left(\frac{A'}{1 - A'}\right)^2 \mu^2\right) - \frac{2A'}{1 - A'}\left(1 + \left(\frac{A'}{1 - A'}\right)^2 \mu^2\right)$$

$$\left. + A'^2(1 + \mu^2)\right] \tag{33}$$

In deriving Equations 32 and 33, 4th order and higher powers of μ are neglected. For small A, these expressions reduce to Equation (31).

1. Events Selected on the Basis of Range

In this case, the energy definition of the scattered particle is limited by the range straggling and errors in range measurement. For the former quantity, we take $\mu_s = 0.20$ (Appendix VII). The error in range measurements was found to be $\mu_o = 0.08 \pm 0.005$. Since Q depends on μ^2, μ_o is negligible compared to μ_s. From the range energy relationship, $R = 0.3\ T^{1.6}$, we have $\Delta R/R = 1.6\ (\Delta T/T)$. For the events selected on the basis of range, $\mu = 0.20/1.6 = 0.12$. From Eq. 31 and this value of μ, the resolution correction becomes four percent.

2. Events Selected on the Basis of Angle

In this case, μ is to be calculated from the error in the scattering angle, $\Delta\theta$. The relationship between these two quantities is (Appendix IX, Eq. 45):

$$\mu^2 = \left\langle \frac{\Delta T^2}{T^2} \right\rangle = (4 \csc 2\theta)^2 \langle \Delta\theta^2 \rangle \tag{34}$$

The problem is to determine $\Delta\theta$ from the errors in δ and a, (Appendix V) for a fixed θ. In Appendix V the relationship, $\cos\theta = \cos\delta/\sqrt{1 + a^2}$, is derived. It follows that:

$$\Delta\theta = \operatorname{ctn}\theta \tan\delta\ \Delta\delta + \frac{\sqrt{\cos^2\delta - \cos^2\theta \cos^2\theta}}{\cos^2\delta \sin\theta}\ \Delta a \tag{35}$$

Squaring Eq. 35 we take the average, recalling $\Delta\delta$ and Δa are independent.

$$\langle \Delta\theta^2 \rangle = \operatorname{ctn}^2\theta\ \langle \tan^2\delta \rangle \cdot \langle \Delta\delta^2 \rangle + \left[\frac{\cos^4\theta}{\sin^2\theta} \langle \sec^2\delta \rangle - \frac{\cos^6\theta}{\sin^2\theta} \langle \sec^4\delta \rangle \right] \cdot \langle \Delta a^2 \rangle \tag{36}$$

From Figure 16

$$\tan\theta \sin\phi = \tan\delta \tag{37}$$

Squaring and taking averages we have:

$$\tan^2\theta \ \langle \sin^2\phi \rangle = \langle \tan^2\delta \rangle$$

Assuming azimuthal symmetry:

$$\langle \tan^2\delta \rangle = \frac{1}{2}\tan^2\theta \tag{38}$$

Similarly:

$$\langle \sec^2\delta \rangle = \langle \tan^2\delta \rangle + 1 = \frac{1}{2}\tan^2\theta + 1 \tag{39}$$

From Eq. 37 we obtain:

$$\tan^4\theta \sin^4\phi = \tan^4\delta$$

Taking averages we have:

$$\langle \tan^4\delta \rangle = \frac{3}{8}\tan^4\theta$$

Hence:

$$\langle \sec^4\delta \rangle = \frac{3}{8}\tan^4\theta + \tan^2\theta + 1 \tag{40}$$

Substituting Equations 38, 39 and 40 into 36 we have:

$$\langle \Delta\theta^2 \rangle = \frac{\langle \Delta\delta^2 \rangle}{2} + F(\theta) \cdot \langle \Delta a^2 \rangle \tag{41}$$

where:

$$F(\theta) = \cos^2\theta \left(\frac{1}{2} - \frac{3}{8}\sin^2\theta\right) \tag{42}$$

The error in δ was measured and found to be:

$$\langle \Delta\delta^2 \rangle = 0.583 \text{ degs.}^2 = 1.77 \times 10^{-4} \text{ rad.}^2$$

The error in a, corresponding to an error ΔD in depth measurement is:

$$\langle \Delta a^2 \rangle = \frac{a^2}{D^2} \langle \Delta D^2 \rangle = \frac{S^2}{L_\theta{}^2} \langle \Delta D^2 \rangle$$

$\langle D^2 \rangle$ is found to be 0.056 (microns)^2. With these measured values of $\langle \Delta \delta^2 \rangle$, $\langle \Delta D^2 \rangle$, and S^2, the L_θ's used in angle measurements, Equations (31), (32), (33), (34), (41), and (42), the ratio $\frac{\sigma}{\Omega}$ is calculated (Table I).

APPENDIX IX

Calculation of the Effects of Range Straggling and Errors in Range and Angle Measurements on the Data of Figure 8

Let:
- μ_s = fractional standard deviation of the range straggling
- μ_o = fractional standard deviation of the observer error in range measurements
- μ_θ = fractional standard deviation in range due to errors in angle measurements
- μ_t = fractional standard deviation of the observed distribution in range (Figure 8).

Since μ_s, μ_o, and μ_θ are independent: $\mu_t^2 = \mu_s^2 + \mu_o^2 + \mu_\theta^2$ (43)

The standard deviation of the range straggling of electrons is $\mu_s = 0.20$ (Appendix VII). The standard deviation of the observer error was found to be $\mu_o = 0.08 \pm 0.005$. From these quantities and knowledge of μ_t, the error in angle measurements can be determined by solving for μ_θ in Equation 43.

The relationship between the error in range and the error in energy is obtained from the range-energy relation, Equation 12.

Thus: $\Delta R/R = 1.6 \times \Delta T/T$ (44)

Differing Equation 11 gives:

$$\Delta T/T = -4 \csc(2\theta)\, \Delta\theta \qquad (45)$$

Combining Equations 44 and 45:

$$\mu_\theta^2 = \left\langle \frac{\Delta R^2}{R^2} \right\rangle = (1.6)^2 \left\langle \frac{\Delta T^2}{T^2} \right\rangle = 16\,(1.6)^2 \csc^2(2\theta)\, \langle \Delta\theta^2 \rangle \qquad (46)$$

The calculated fractional standard deviation (with their probable errors) for the two sets of data of Figure 8 are:

$\mu_t^- = 0.65 \pm 0.08$ (e-e collisions, 27 events)

$\mu_t^+ = 0.63 \pm 0.04$ (p-e collisions, 86 events)

Substituting either of these quantities with the known values of μ_s and μ_o, and the mean value of the angle ($\bar{\theta} = 65^o$) into Equation (43), we obtain, with the aid of Equation (46), the average value of the standard deviation of θ.

$$\langle \langle \Delta\theta^2 \rangle^{1/2} \rangle = 3.5^o$$

This is a reasonable result for the range of angles in Figure 8.

The ratio: $\mu_t^- / \mu_t^+ = 1.02 \pm 0.05$ indicates that there is no significant difference in the spread of the two sets of points. Thus, the inelastic scattering is not detected within the probable error of 5 percent.

The standard error of the mean range as determined from the weighted means of μ_t^+ and μ_t^- is: $\frac{0.63}{\sqrt{113}} = 6$ percent.

APPENDIX X

Calculation of the Rutherford Scattering in Terms of the Projected Angle

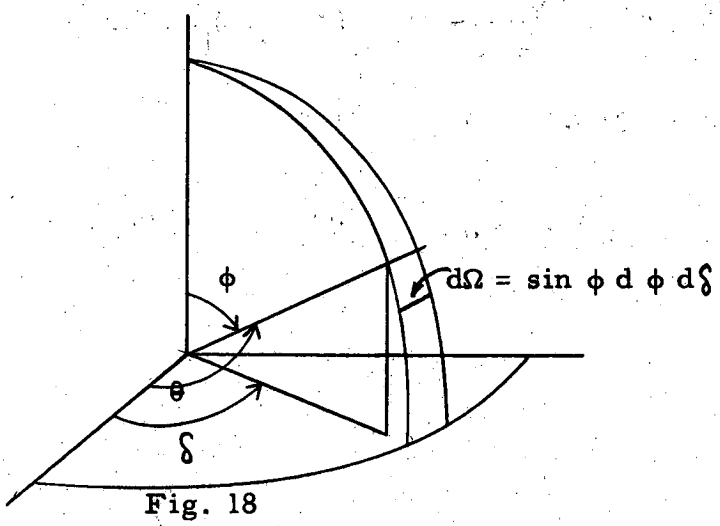

Fig. 18

The Rutherford scattering cross section is:

$$\sigma(\theta)\, d\Omega = A \csc^4 \frac{\theta}{2}\, d\Omega \qquad (47)$$

$$= \frac{4A}{(1 - \cos\theta)^2}\, d\Omega$$

where $d\Omega$ is the element of solid angle

From Figure 18:

$$\cos\phi = \cos\delta \sin\theta$$

Eq. 47 becomes:

$$\sigma(\theta)\, d\Omega = w(\phi\delta) \sin\phi\, d\phi = \frac{4A\, d\delta \sin\phi\, d\phi}{(1 - \cos\delta \sin\phi)^2}$$

$$w(\delta)\, d\delta = 4A\, d\delta \int_{\phi=0}^{\pi} \frac{\sin\phi\, d\phi}{(1 - \cos\delta \sin\phi)^2}$$

Let $x = 1 - \cos\delta \sin\phi$

$$w(\delta)\, d\delta = -\frac{8A\, d\delta}{\cos\delta} \int_{x=1}^{1-\cos\delta} \frac{(1-x)\, dx}{x^2 \sqrt{\cos^2\delta - (1-x)^2}}$$

$$w(|\delta|)\, d\delta = \frac{16A\, d\delta}{\sin^2\delta} \left[1 + (\pi - |\delta|) \operatorname{ctn}|\delta|\right] \tag{15}$$

The integrated cross section is:

$$\int_{|\delta|}^{\pi} w(|\delta|)\, d\delta = 8A \left[\operatorname{ctn}|\delta| + (\pi - |\delta|) \csc^2\delta\right] \tag{48}$$

APPENDIX XI

Calculation of the Ratio $r = \int_{\delta}^{\pi} w(|\delta|)\, d \;/ \int_{\theta}^{\pi} \sigma(\theta)\, d\Omega$

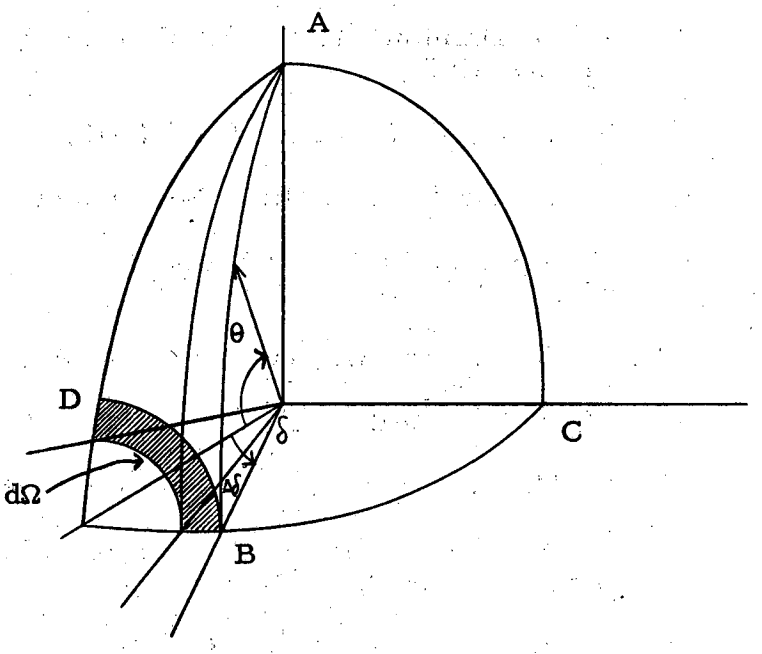

From the integration of the Rutherford cross section (Eq. 47) and Eq. 48 the ratio r is found to be:

$$r = \frac{4\pi A \left[\frac{1}{\sin^2 \frac{\theta}{2}} - 1\right]}{8A \left[\operatorname{ctn} |\delta| + (\pi - |\delta|) \csc^2 \delta\right]}$$

The limit of r ($|\delta| = \theta$) as $\theta \longrightarrow 0$ is 2. It follows that the number of events in the lune ABC (Fig. 19) is equal to the number of events through the area ADB. In a similar way one can also show that the ratio

$$\sigma(\theta)\, \Delta\Omega / w(|\delta|)\, \Delta\delta$$

approaches 2 for $\theta = \delta$ in the limit of small angles. Because these ratios are independent of angle the abscissa of Fig. 13 may be directly interpreted as either δ or θ.

REFERENCES

1. H. Yagoda and N. Kaplan, Phys. Rev. 73, 634 (1948).
2. C. Dilworth, G. Occhialini and L. Vermaesen, Bull. Cen. Phys. Nuc., Brussels (1950).
3. A. D. Dainton, A. R. Gattiker and W. O. Lock, Phil. Mag. 42, 396 (1951).
4. N. Bohr, Phil. Mag. 25, 10 (1913), 30, 328 (1915).
5. N. F. Mott, Proc. Roy. Soc. (London) A126, 259 (1930).
6. C. Møller, Zeit. f. Physik 70, 786 (1931), Ann. d. Physik 14, 531 (1933).
7. K. C. Kar and C. Basu, Ind. J. Phys. 18, 223 (1944).
8. W. Bothe, Zeit. f. Physik 12, 117 (1922).
9. C. T. R. Wilson, Proc. Roy. Soc. (London) 104, 1, 192 (1923).
10. E. J. Williams and F. R. Terroux, Proc. Roy. Soc. (London) A126, 289 (1929).
11. E. J. Williams, Proc. Roy. Soc. (London) A128, 459 (1930).
12. E. J. Williams, Proc. Roy. Soc. (London) A130, 328 (1930).
13. F. C. Champion, Proc. Roy. Soc. (London) A137, 688 (1932).
14. G. Hornbeck and I. Howell, Proc. Am. Phil. Soc. 84, 33 (1941).
15. P. E. Shearin and T. E. Pardue, Proc. Am. Phil. Soc. 85, 243 (1942).
16. L. A. Page and W. M. Woodward, Phys. Rev. 79, 228 (1950).
17. G. Groetzinger, L. B. Leder, F. L. Ribe and M. J. Berger, Phys. Rev. 79, 454 (1950).
18. F. C. Gilbert, C. E. Violet and W. H. Barkas, Phys. Rev. 81, 656 (1951).
19. M. B. Scott, A. O. Hanson and E. M. Lyman, Phys. Rev. 84, 638 (1951).
20. W. C. Barber, G. E. Becker and E. L. Chu, Phys. Rev. 85, 774 (1952).

21. H. J. Bhabha, Proc. Roy. Soc. (London) A154, 195 (1936).

22. Ho Zah-Wei, Phys. Rev. 70, 224 (1946), Comp. Rend. 226, 1083 (1948).

23. W. H. Barkas, R. W. Deutsch, F. C. Gilbert and C. E. Violet, Phys. Rev. 86, 59 (1952), Phys. Rev. 88, 1435 (1952).

24. R. R. Roy and L. Groven, Phil. Mag. 43, 1291 (1952).

25. Von O. Ritter, C. Lieseberg, H. Maier-Leibnitz, A. Popkow, K. Schmeiser and W. Bothe, Zeit. f. Naturforsch. 6a, 243 (1951).

26. G. R. Hoke, Phys. Rev. 87, 285 (1952).

27. H. A. Howe and K. R. MacKenzie, Pasadena Meeting, Am. Phys. Soc., Dec. (1952).

28. L. Voyvodic and E. Pickup, Phys. Rev. 85, 91 (1952).

29. M. Weissbluth, Univ. of Calif. Rad. Lab., UCRL-568 (1950).

30. B. Zajac and M. Ross, Nature 164, 311 (1949).

31. A. Bonetti and G. Tomasini, Nuovo Cimento 8, 693 (1951).

32. Mott and Massey, Theory of Atomic Collisions, Oxford (1949) p. 368.

33. G. Occhialini, Como Congress (Nuovo Cimento, Suppl. 6, 377 (1949)).

34. D. R. Corson and M. R. Keck, Phys. Rev. 79, 209 (1950).

35. P. H. Fowler, Phil. Mag. 41, 169 (1950).

36. U. Camerini, P. H. Fowler, W. O. Lock and H. Muirhead, Phil. Mag. 41, 413 (1950).

37. E. Pickup and L. Voyvodic, Phys. Rev. 80, 89 (1950); L. Voyvodic, Bristol Conference (1951).

38. T. Bowen and F. X. Roser, Phys. Rev. 83, 689 (1951).

39. I. B. McDiarmid, Phys. Rev. 84, 851 (1951).

40. A. H. Morrish, Phil. Mag. 43, 533 (1952).

41. S. G. Gosh, G. M. D. B. Jones and J. G. Wilson, Proc. Phys. Soc. 65, 68 (1952).

42. B. Stiller and M. Shapiro, Phys. Rev. 87, 682 (1952).

43. H. Bethe, Zeit. f. Physik 76, 293 (1932), Ann. d. Physik 5, 325 (1930).

44. F. Block, Ann. d. Physik 16, 285 (1933), Zeit. f. Physik 81, 363 (1933).

45. E. J. Williams, Proc. Roy. Soc. (London) A135, 108 (1932), A139, 163 (1933).

46. E. Fermi, Phys. Rev. 57, 485 (1940).

47. G. C. Wick, Ric. Scient. 11, 273 (1940), 12, 858 (1941), Nuovo Cimento 1, 302 (1943).

48. O. Halpern and H. Hall, Phys. Rev. 57, 459 (1940), 73, 477 (1948).

49. A. Bohr, Det. Kgl. Dans. Vid. Sels. 24, n. 19 (1948).

50. M. Schönberg, Bull. Cent. Phys. Nucl. Brus. n 20 (1948).

51. M. Schönberg, Nuovo Cimento 8, 159 (1951), 9, 210 (1952), 9, 372 (1952).

52. R. M. Sternheimer, Phys. Rev. 88, 851 (1952).

53. M. Huybrechts and M. Schönberg, Nuovo Cimento 9, 764 (1952).

54. P. G. Hoel, "Introduction to Mathematical Statistics," Wiley (1947) p. 152.

55. E. J. Williams, Proc. Roy. Soc. 169, 153 (1939); Phil. Mag. 40, 1250 (1949).

56. B. Rossi and K. I. Greisen, Rev. Mod. Phys. 13, 240 (1941).

57. G. Molière, Zeits. f. Naturforsch. 2a, 133 (1947), 3a, 78 (1948).

58. Y. Goldschmidt-Clermont, Nuovo Cimento 7, 331 (1950).

59. S. A. Colgate and F. C. Gilbert, Phys. Rev. 89, 790 (1952).

60. H. J. Bramson, A. M. Seifert, and W. W. Havens, Phys. Rev. 88, 304 (1952).

61. P. A. M. Dirac, Proc. Camb. Phil. Soc. 26, 361 (1930).

62. W. Heitler, The Quantum Theory of Radiation, Oxford (1944) p. 200.

63. W. Heitler, The Quantum Theory of Radiation, Oxford (1944) p. 208.

64. W. Heitler, The Quantum Theory of Radiation, Oxford (1944) p. 209.

65. H. R. Crane and J. Halpern, Phys. Rev. 55, 838 (1939).

66. F. Barendregt, J. Griffioen and G. J. Sizoo, Physica 7, 860 (1940).

67. J. R. Feldmeier and G. B. Collins, Phys. Rev. 58, 200 (1940).

68. N. Feather and J. V. Dunworth, Proc. Camb. Phil. Soc. 34, 435 (1938).

69. H. Staub, Helv. Phys. Acta 9, 306 (1939).

70. M. R. Cleland, W. R. Konneker and A. L. Hughes, Phys. Rev. 79, 229 (1950).

71. J. E. Hooper, D. T. King and A. H. Morrish, Phil. Mag. 42, 304 (1951), 43, 853 (1952).

72. N. J. Shiren and R. F. Post, Phys. Rev. 86, 617 (1952).

73. H. L. Bradt, M. F. Kaplon and B. Peters, Helv. Phys. Acta 23, 43 (1950).

74. G. P. S. Occhialini, Nuovo Cimento Supp. 6, 3, 413 (1949).

75. M. Camac, Phys. Rev. 88, 745 (1952).

76. H. J. Bhabha, Proc. Roy. Soc. (London) A152, 559 (1935).

77. W. Heitler, The Quantum Theory of Radiation, Oxford (1944) p. 172.

78. D. R. Corson, Phys. Rev. 80, 303 (1950).

79. H. W. Lewis, Phys. Rev. 85, 20 (1952).

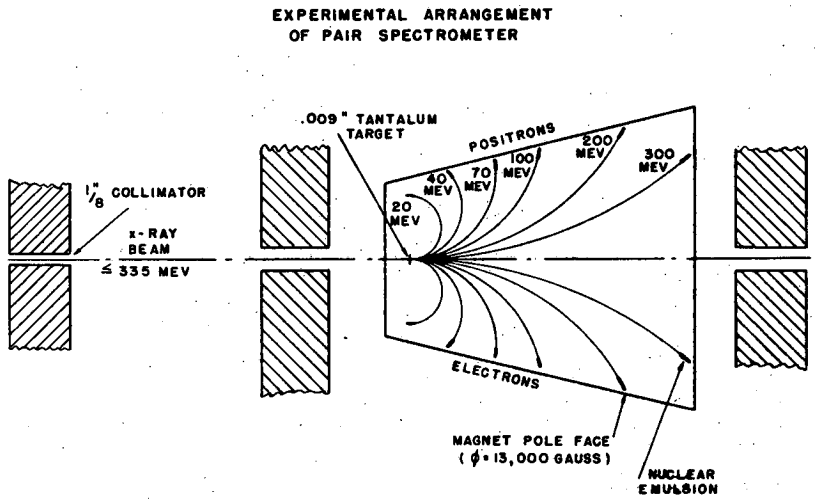

Fig. 1

Arrangement of the photographic emulsions in the magnetic field of the synchrotron pair spectrometer.

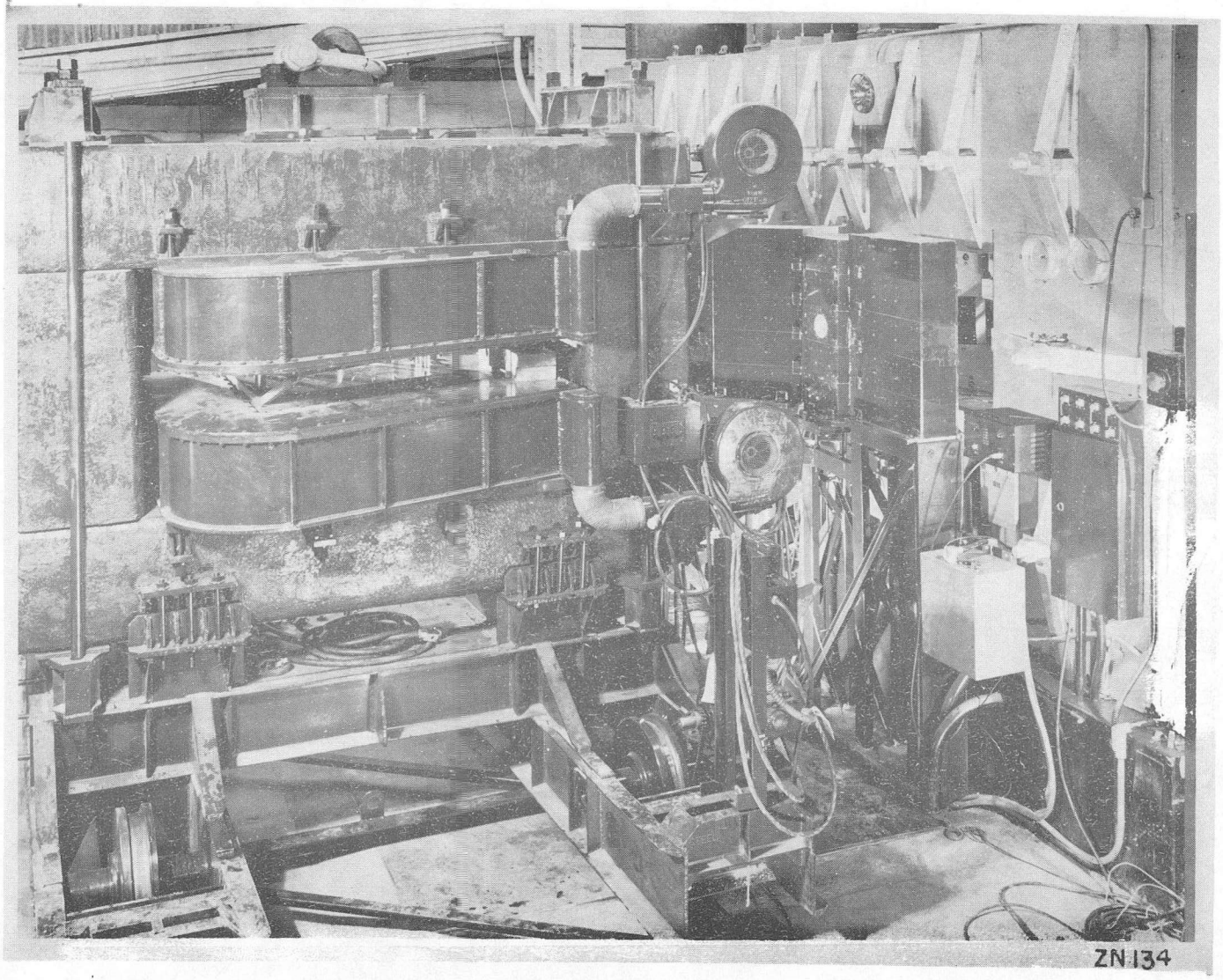

Fig. 2

Photograph showing pair spectrometer in place behind synchrotron.

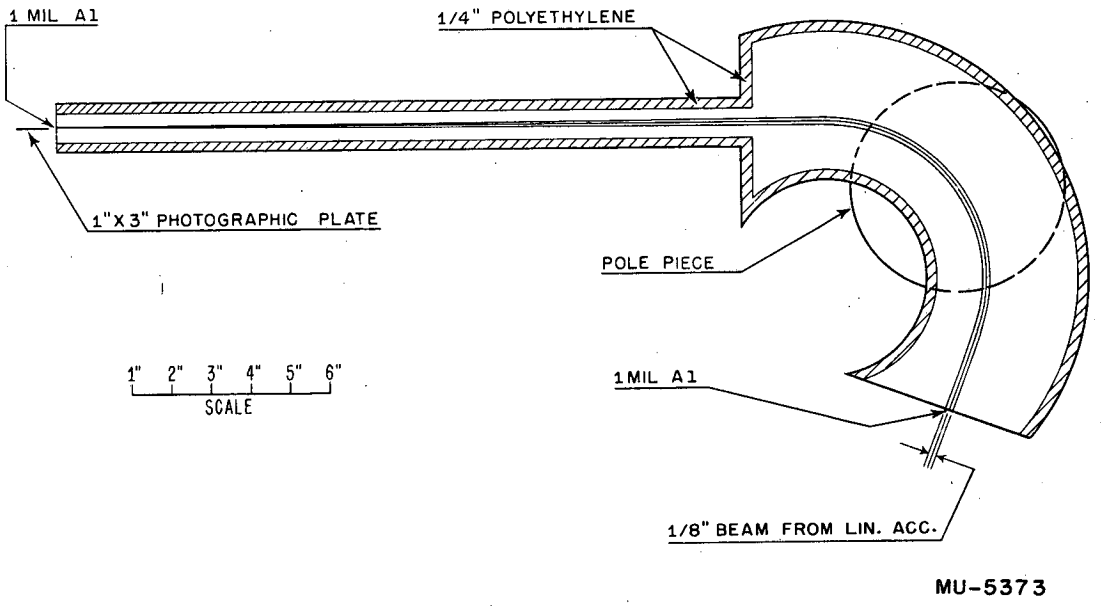

Fig. 3

Experimental arrangement for electron linear accelerator exposures.

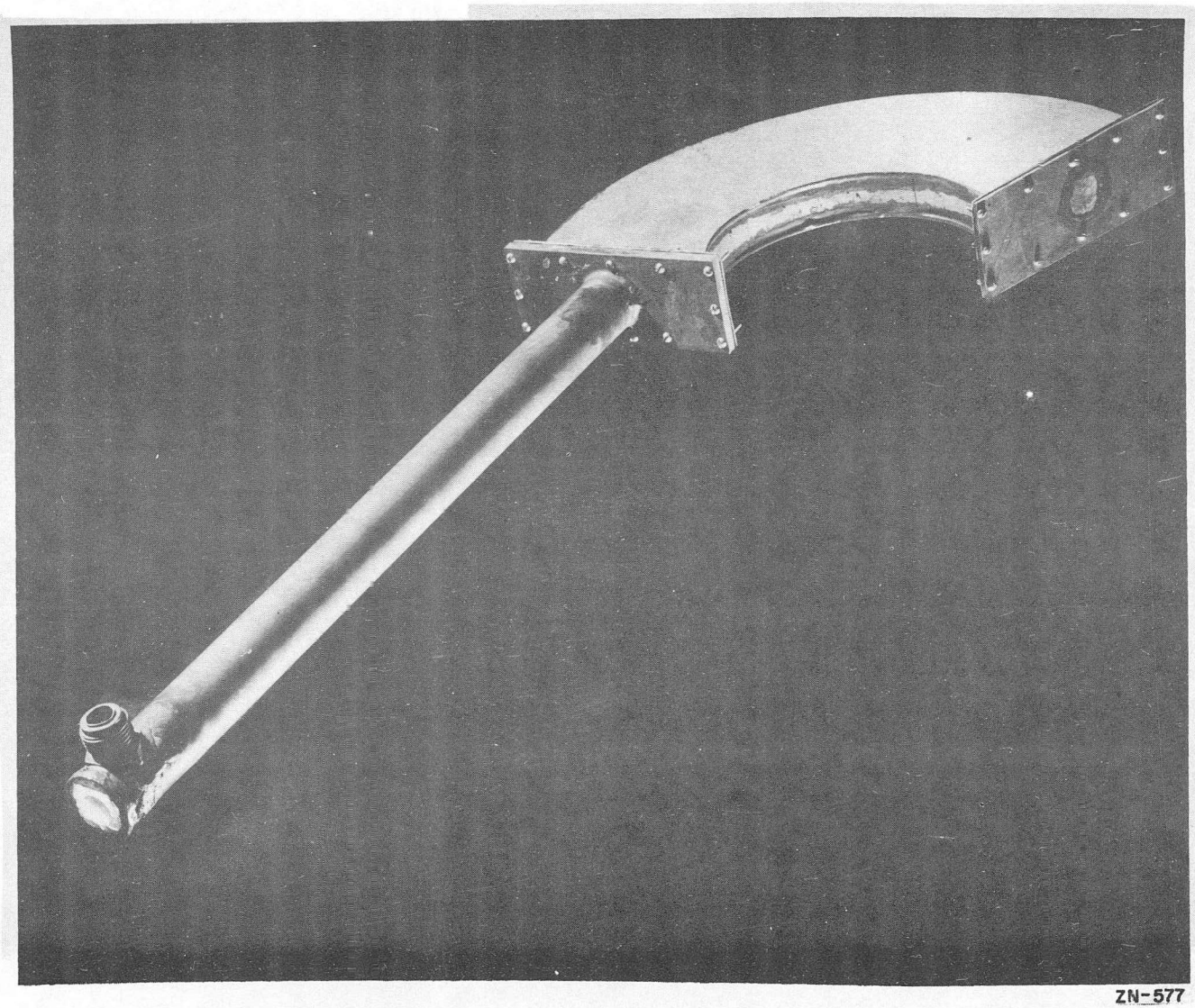

Fig. 4

Photograph of the analyzing channel used in the analysis of the electron linear accelerator beam.

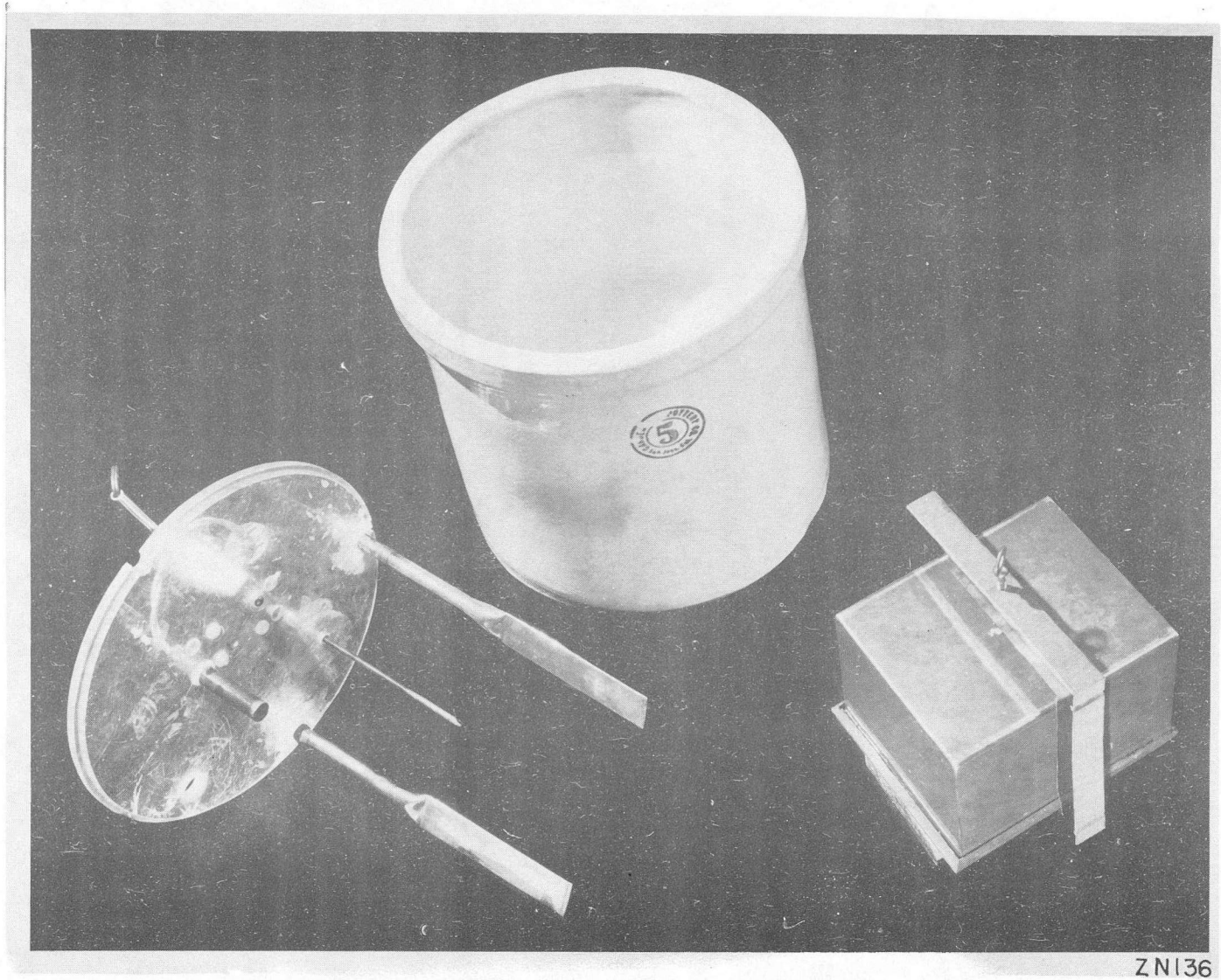

Fig. 5

Eradication apparatus consisting of (1) porcelain crock for water bath, (2) plastic cover containing heating elements, thermostat and thermometer, (3) sealed box.

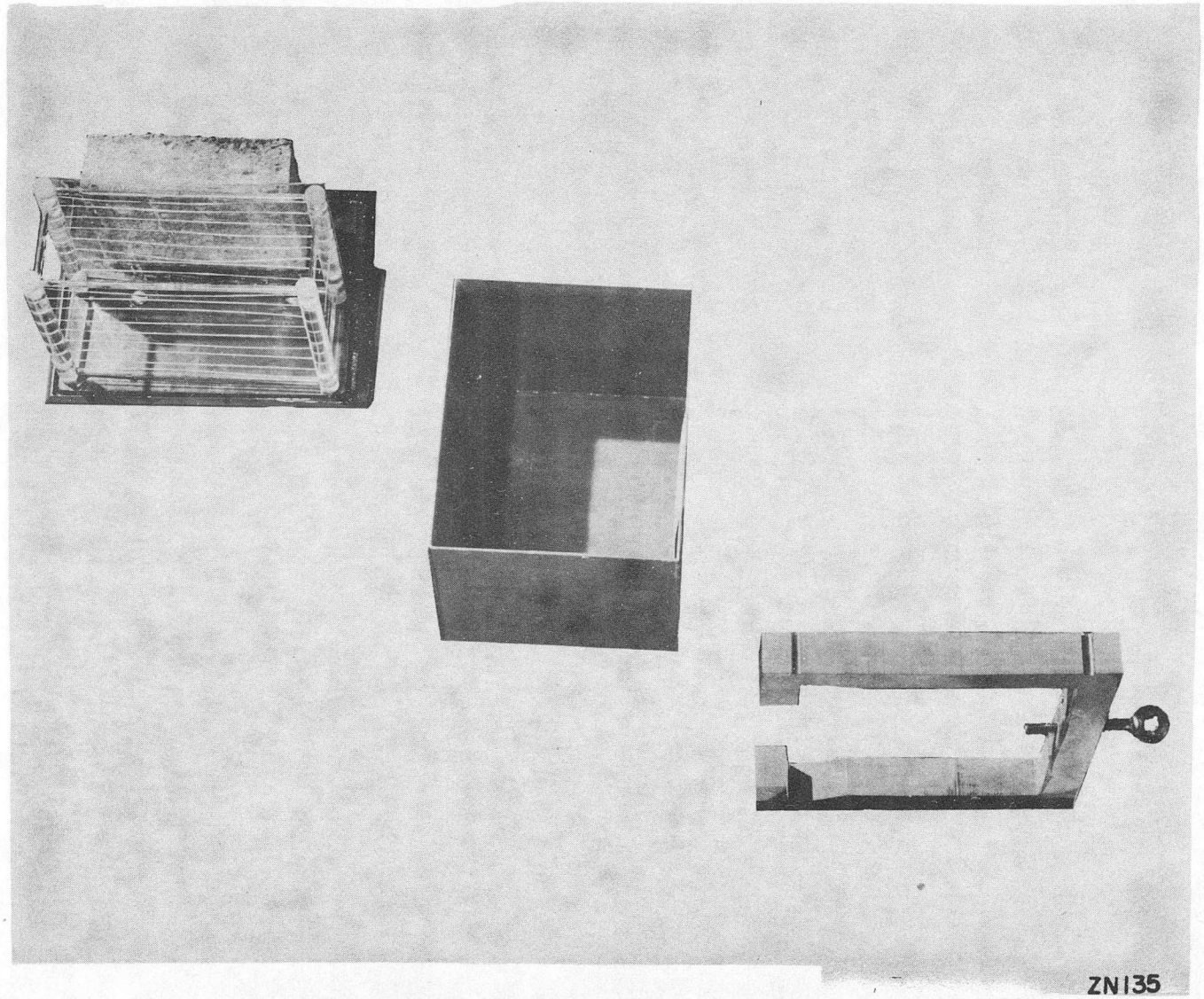

Fig. 6

Contents of box: (1) platform holding lucite frame and sponge, (2) cover, (3) cover clamp.

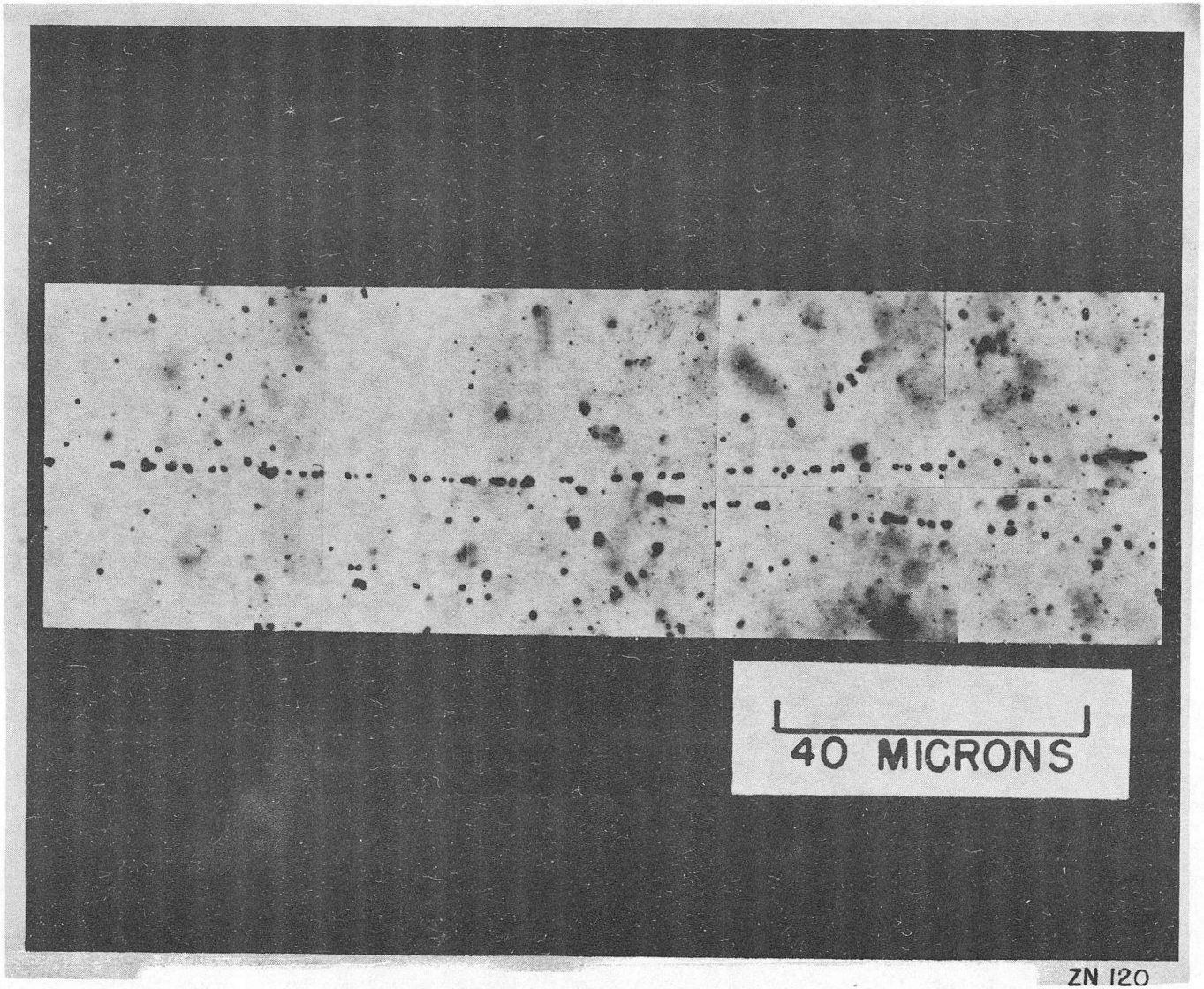

Fig. 7

Microphotograph mosaic of a positron-electron collision of large energy transfer initiated by a ~185 Mev primary positron. The angles of scatter are 9° and 2°.

TABLE I

Calculation of the Resolution Correction to the Electron-Electron and Positron-Electron Scattering Cross Sections

~174 Mev Primary Energy

Energy Interval (Mev)	θ_{Ti}	$F(\theta_{Ti})$	$L_\theta(\mu)$	$\langle \Delta a^2 \rangle \times 10^3$	$F(\theta)\cdot\langle \Delta a^2 \rangle \times 10^3$	$\langle \Delta\theta^2 \rangle \times 10^3$	$16 \csc^2 2\theta$	$\mu^2 \times 10^2$	$\frac{\sigma}{\Omega}$
0.4- 0.8	53.0°	0.157	10	3.50	0.550	0.638	14.8	0.944	0.980
0.8- 1.6	42.5°	0.179	20	0.875	1.56	1.64	17.6	2.89	0.926
1.6- 3.2	35.0°	0.252	20	0.875	2.20	2.28	18.0	4.10	0.893
3.2- 6.4	24.5°	0.361	30	0.389	1.40	1.48	20.8	3.08	0.917
6.4-12.8	17.5°	0.424	30	0.389	1.65	1.73	48.6	8.42	0.800
12.8-25.6	12.5°	0.460	40	0.219	1.00	1.08	89.8	9.70	0.775
25.6-51.2	8.5°	0.480	40	0.219	1.05	1.13	187.0	21.1	0.606

~39 Mev Primary Energy

	Interval (A)	θ_{Ai}	$F(\theta_{Ai})$	$L_\theta(\mu)$	$\langle \Delta a^2 \rangle \times 10^5$	$F(\theta_{Ai})\cdot\langle \Delta a^2 \rangle \times 10^4$	$\langle \Delta\theta^2 \rangle \times 10^4$	$16 \csc^2 2\theta$	$\mu^2 \times 10^2$	$\frac{\sigma}{\Omega}$
(e-e)	0.2-0.5	16.0°	0.435	50	1.40	6.09	6.97	57.1	3.98	0.934
(p-e)	0.2-0.5	15.5°	0.440	50	1.40	6.16	7.04	60.3	4.24	0.892

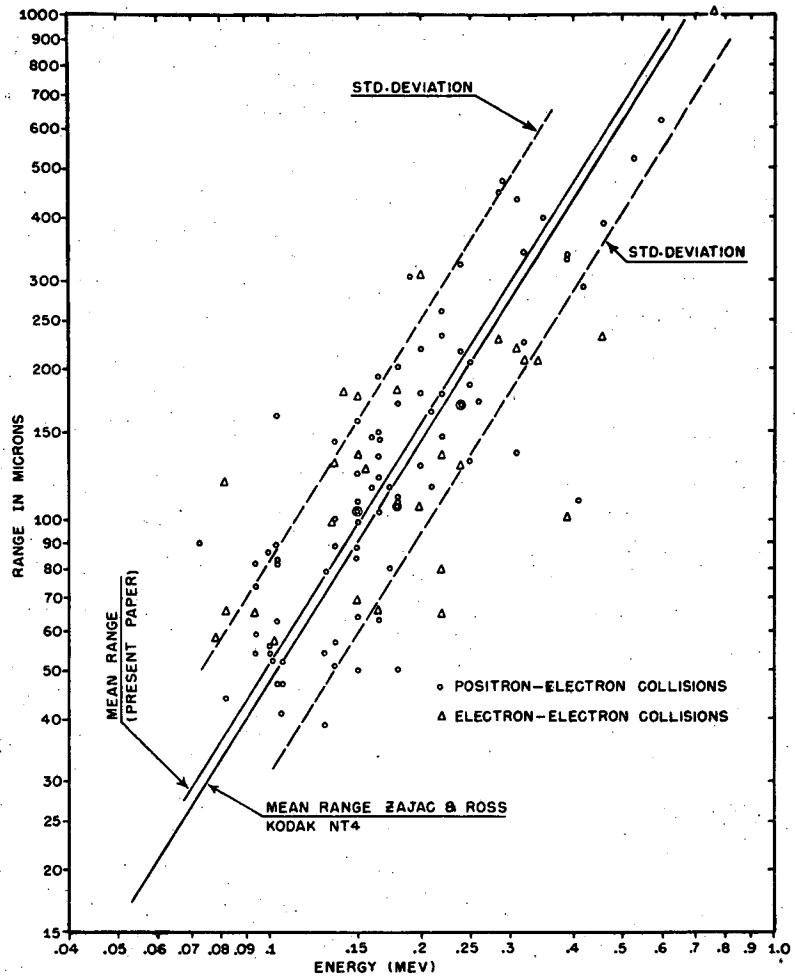

ELECTRON RANGE-ENERGY RELATION.
ILFORD G-5

MU-5378

Fig. 8

TABLE II

Electron-Electron Scattering

16.4 ± 21 Mev Primary Energy

Energy Interval (Mev)	Total Track Length (cm)	T_i Mev	ΔN_θ	ΔN_R	Corrections: Efficiency	Corrections: Resolution	Exp'tl cross section bns/Mev	exp't / Møller	P. E.
0.03 - 0.05	30.76	0.0397		98	1.143	0.955	163	0.95	0.12
0.05 - 0.1		0.0708		67			44.6	0.87	0.12
0.1 - 0.2		0.141	71	73			12.8	1.00	0.07
0.2 - 0.4		0.282	33	35			3.06	0.96	0.11
0.4 - 0.8		0.566	13	9		0.980	0.584	0.73	0.22
0.8 - 1.6	51.70	1.13	4		1.015	0.926	8.50×10^{-2}	0.42	0.33
1.6 - 3.2		2.26	4			0.893	4.09×10^{-2}	0.82	0.33
3.2 - 6.4		4.55	2			0.917	1.05×10^{-2}	0.84	0.47
6.4 - 12.8		9.06	3			0.800	6.88×10^{-3}	2.21	0.39
12.8 - 25.6		18.1	1			0.776	1.11×10^{-3}	1.42	0.67

36.1 ± 3.6 Mev Primary

ΔA	Total Track Length (cm)	A_i	ΔN_θ	Corrections: Efficiency	Corrections: Resolution	Exp'tl cross section bns	exp't / Møller	P. E.
0.2-0.5	109.6	0.31	4	1.125	0.934	1.19×10^{-1}	1.19	0.35

TABLE III

Positron-Electron Scattering

185 ± 37 Mev Primary Energy

Energy Interval (Mev)	Total Track Length (cm)	T_i (Mev)	ΔN_θ	ΔN_R	Corrections: Efficiency	Corrections: Resolution	Exp'tl cross section bns/Mev	exp't / Bhabha	P. E.
0.03- 0.05	16.6	0.0397		54	1.143		164	0.96	0.13
0.05- 0.01		0.0708		59			72.0	1.40	0.13
0.1 - 0.2		0.141	131	132		0.955	11.6	0.91	0.05
0.2 - 0.4		0.282	60	62		2.73	2.73	0.86	0.08
0.4 - 0.8		0.566	25	23		0.980	0.567	0.71	0.14
0.8 - 1.6		1.13	9		1.015	0.926	9.63×10^{-2}	0.48	0.24
1.6 - 3.2	102.6	2.26	7			0.893	3.61×10^{-2}	0.74	0.25
3.2 - 6.4		4.55	8			0.917	2.12×10^{-2}	1.81	0.24
6.4 -12.8		9.06	2			0.800	2.31×10^{-3}	0.81	0.47
12.8 -25.6		18.1	1			0.776	5.61×10^{-4}	0.84	0.67
25.6 -51.2		33.5	1			0.606	2.19×10^{-4}	1.27	0.67

42.9 ± 4.3 Mev Primary Energy

ΔA	Total Track Length (cm)	A_i	ΔN_θ	Corrections: Efficiency	Corrections: Resolution	Exp'tl cross section bns	exp't / Bhabha	P. E.
0.2-0.5	205.3	0.35	3	1.125	0.892	4.57×10^{-2}	1.20	0.40

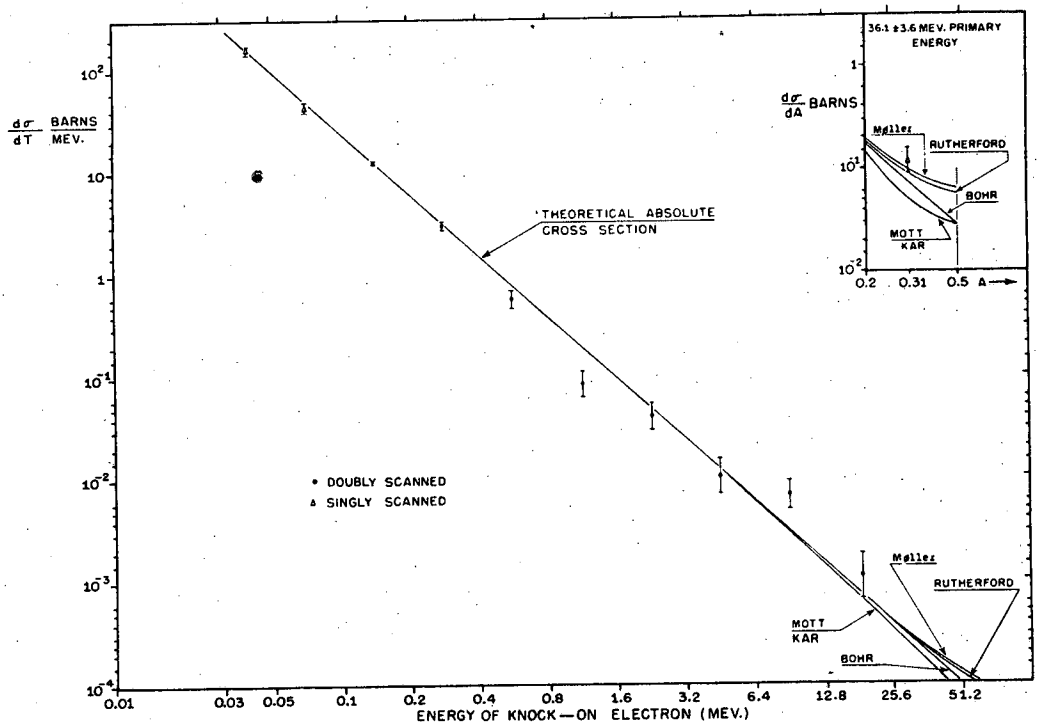

DIFFERENTIAL SCATTERING CROSS SECTION ELECTRON—ELECTRON SCATTERING
164 ± 21 MEV. PRIMARY ENERGY
MU-5377

Fig. 9

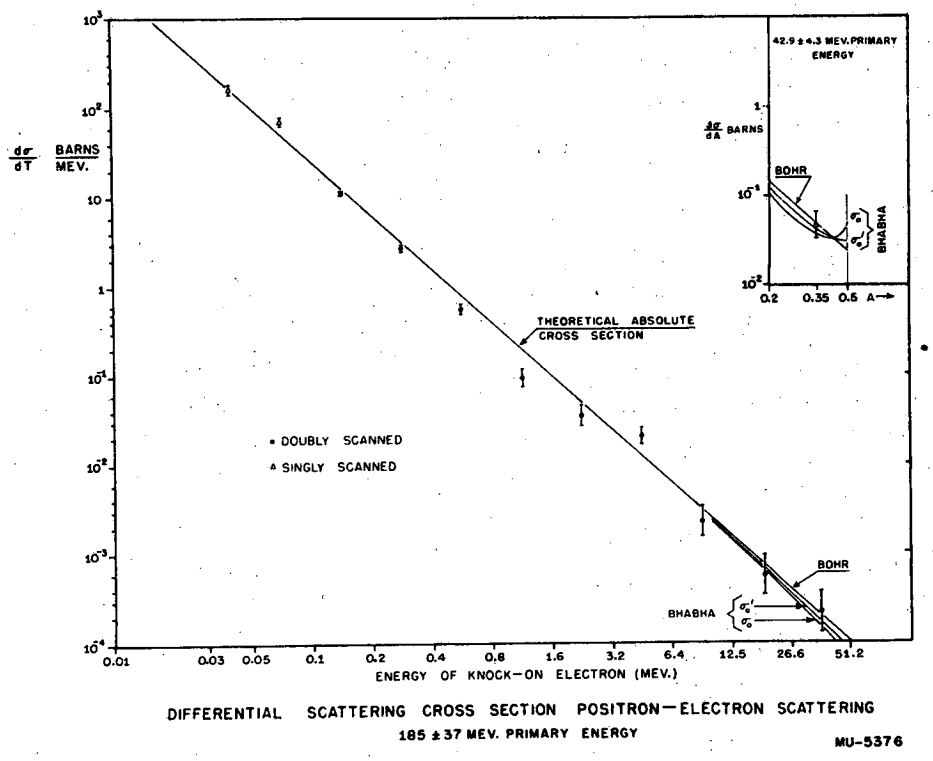

DIFFERENTIAL SCATTERING CROSS SECTION POSITRON—ELECTRON SCATTERING
185 ± 37 MEV. PRIMARY ENERGY
MU-5376

Fig. 10

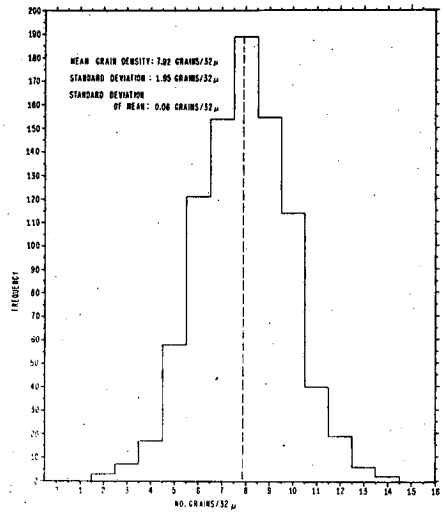

FREQUENCY DISTRIBUTION OF GRAIN COUNTS FOR 2.8 MEV. ELECTRONS.

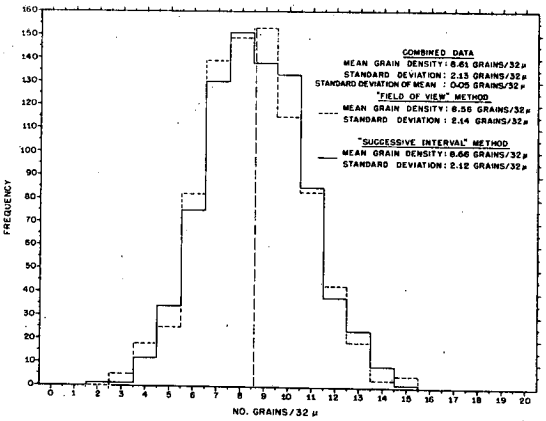

FREQUENCY DISTRIBUTION OF GRAIN COUNTS FOR 293 MEV. ELECTRONS

MU-5379

Fig. 11

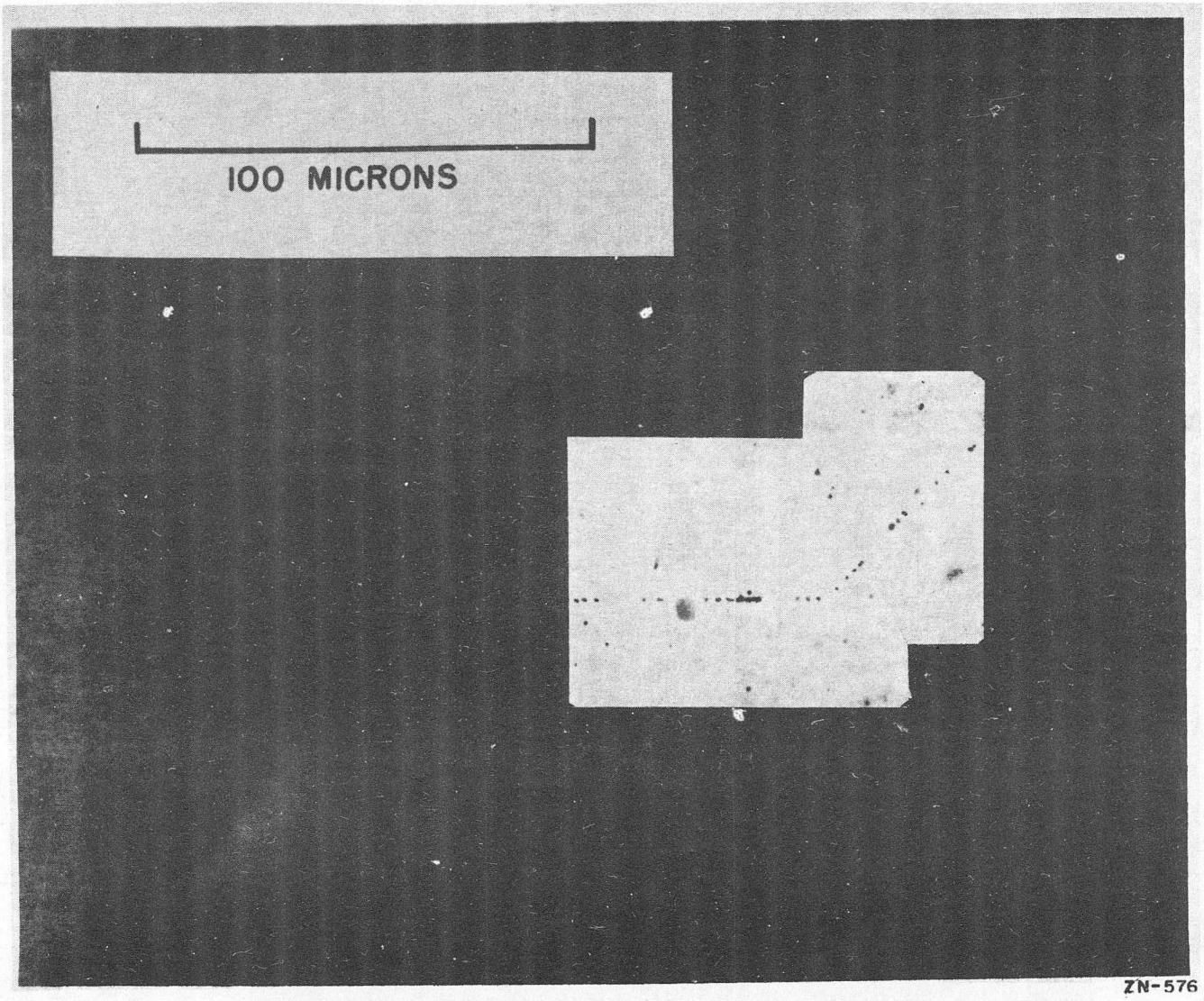

Fig. 12

Microphotograph mosaic of an electron-nuclear scatter. The projected angle is 45 degrees.

TABLE IV

Nuclear Scattering of 36.1 ± 3.6 Mev Electrons and 42.9 ± 4.3 Mev Positrons

$\Delta\delta$ or $\Delta\theta$	No. of events		Primary track length cm		$\frac{\sigma}{\sigma_R}$	
	electron	positron	electron	positron	electron	positron
3.5- 4.5	67	68	162	200	1.08±0.20	1.24±0.24
4.5- 5.5	55	51			1.40±0.28	1.53±0.30
5.5- 6.5	23	20			0.95±0.27	1.00±0.28
6.5- 7.5	19	22			1.32±0.26	1.87±0.37
7.5-10.5	21	17			1.13±0.27	1.08±0.27
10.5-14.5	8	8			0.41±0.12	1.02±0.31
14.5-19.5	16	11	519	557	1.05±0.27	1.02±0.28
19.5-29.5	9	9			0.83±0.25	1.00±0.30
29.5-90.0	4	2			0.61±0.23	0.43±0.21

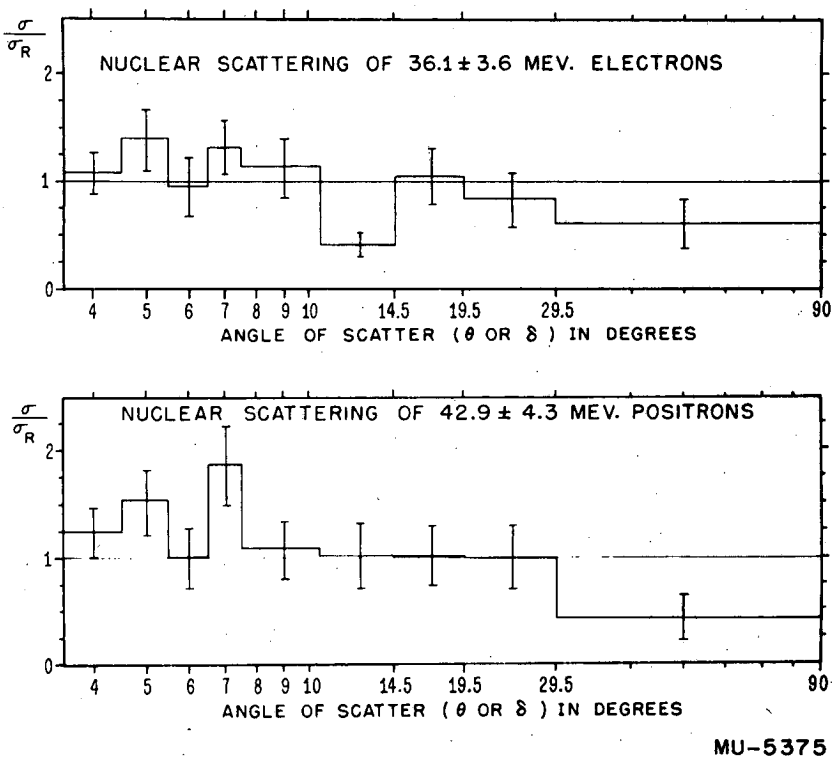
$\frac{\sigma}{\sigma_R}$
NUCLEAR SCATTERING OF 36.1 ± 3.6 MEV. ELECTRONS
2
1
0
4 5 6 7 8 9 10 14.5 19.5 29.5 90
ANGLE OF SCATTER (θ OR δ) IN DEGREES
$\frac{\sigma}{\sigma_R}$
NUCLEAR SCATTERING OF 42.9 ± 4.3 MEV. POSITRONS
2
1
0
4 5 6 7 8 9 10 14.5 19.5 29.5 90
ANGLE OF SCATTER (θ OR δ) IN DEGREES
MU-5375

Fig. 13

TABLE V

Annihilation in Flight of Positrons

Mean Energy Mev	No. of events	Tracklength (cm)	Exp'tl Ann. length and std. error (cm)	Theoretical Ann. length (cm)
185 ± 37	2	102	51 ± 36	243
42.9 ± 4.3	3	200	66 ± 38	76

TABLE VI

Pair Production in the Field of a Nucleus

Mean Primary Energy	No. of events	Track length (cm)	Exp'tl Mean free path and std. error (cm)	Theoretical Mean free path (cm)
200 Mev electron exposure				
164 ± 21 Mev	2	102	51 ± 36	79
300 Mev positron exposure				
288 Mev (calculated)	1	31	31 ± 31	19

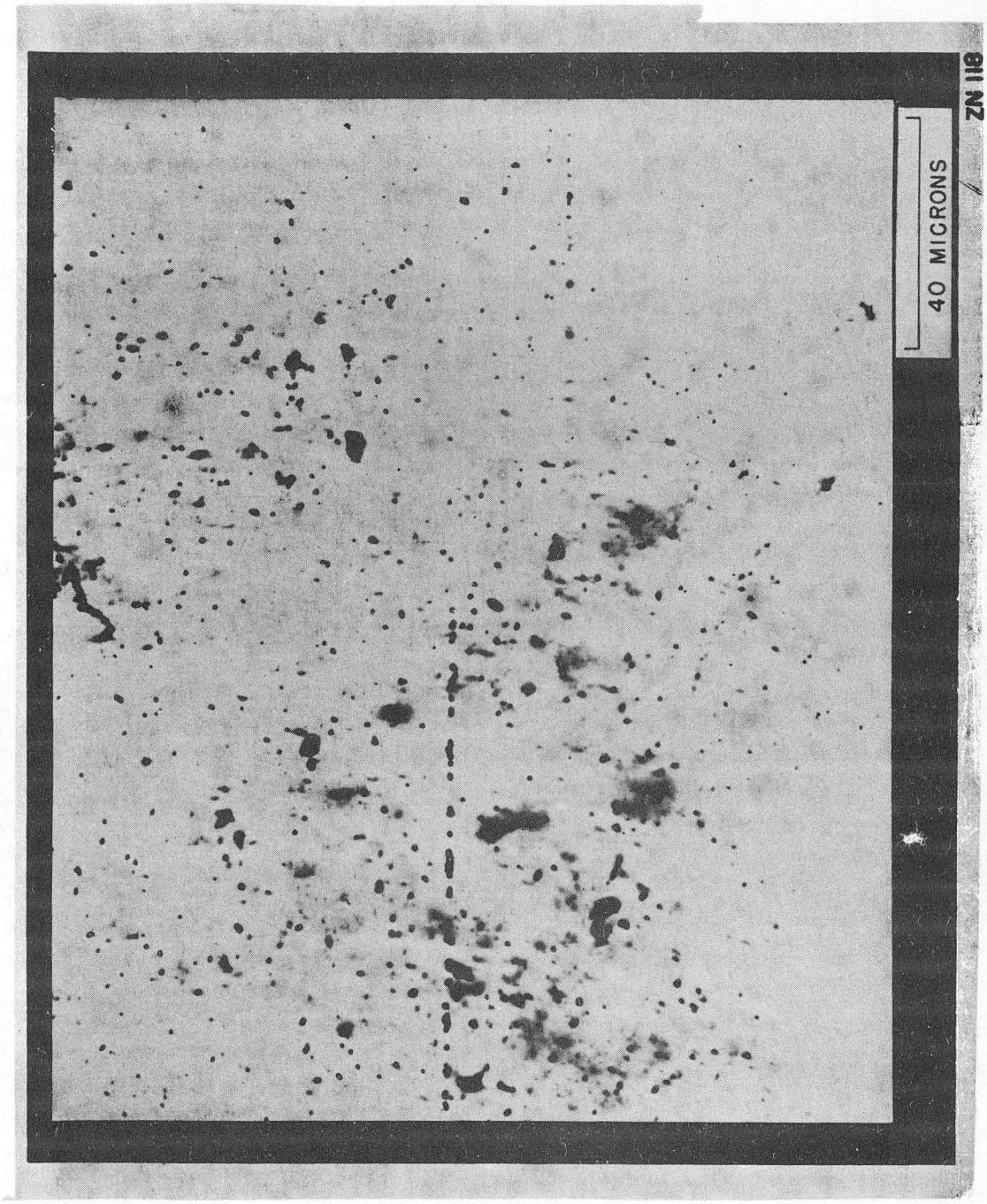

Fig. 14

Microphotograph mosaic of the annihilation in flight of a ~185 Mev positron.

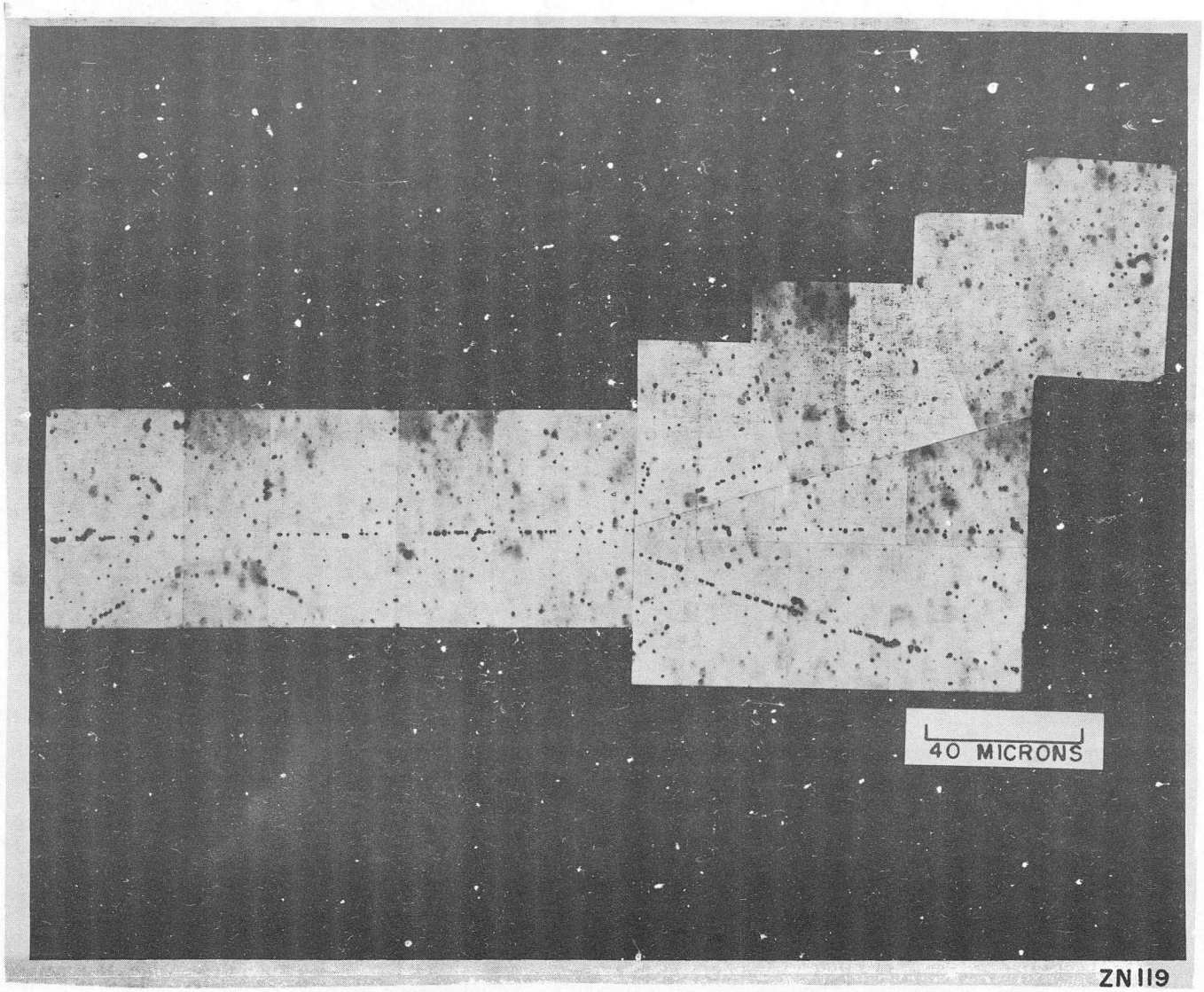

Fig. 15

Microphotograph mosaic of a pair in the field of a nucleus by a ~185 Mev positron.